Aalto University
School of Chemical
Engineering

Patrik Eskelinen

COBALT CATALYST CHARACTERIZATION AND MODIFICATION BY ATOMIC LAYER DEPOSITION FOR FISCHER-TROPSCH SYNTHESIS

Master´s Programme in Chemical, Biochemical and Materials Engineering
Major in Functional Materials

Master's thesis for the degree of Master of Science in Technology
submitted for inspection, Espoo, 2nd of April, 2019.

Supervisor Professor Sami Franssila

Instructor M.Sc. Laura Keskiväli
M.Sc. Niko Heikkinen

Aalto University
School of Chemical
Engineering

Aalto University, P.O. BOX 11000, 00076 AALTO
www.aalto.fi

Abstract of master's thesis

Author Patrik Eskelinen

Title of thesis Cobalt catalyst characterization and modification by atomic layer deposition for Fischer-Tropsch synthesis

Degree Programme Chemical, Biochemical and Materials Engineering

Major Functional Materials

Thesis supervisor Professor Sami Franssila

Thesis advisor(s) / Thesis examiner(s) M.Sc. Laura Keskiväli; M.Sc. Niko Heikkinen

Date 02.04.2019 **Number of pages** 54 **Language** English

Abstract

Fischer-Tropsch synthesis (FTS) is a heterogeneously catalyzed process which produces hydrocarbons from carbon monoxide and hydrogen. FTS is a promising stepping stone to more effectively use available gas resources both fossil and renewable, or to produce petroleum substitutes from industrial sidestreams and captured carbon dioxide converted to carbon monoxide. From the catalysts used in FTS, cobalt-based catalysts are of interest due to their higher activity, heavier product fractions, and natural selectivity towards paraffins as compared to iron-based catalysts.

The tailoring of catalysts produced by commonly used impregnation methods is a means to develop more resilient and selective catalysts. Atomic layer deposition (ALD) is capable of coating very conformal layers in porous catalysts, becoming a useful tool in modifying supported catalysts very precisely. Top-coating by ALD alumina and promotion by ALD platinum are the modifications investigated in this thesis to improve resilience and applying a highly dispersed effective promoter. A roster of characterization methods including X-ray diffraction, electron microscopy, energy dispersive X-ray spectroscopy, X-ray fluorescence, among others are discussed and implemented in this work.

The catalysts studied are composed of silicon doped gamma alumina supported cobalt catalysts with ~30 wt% Co and 0.1 wt% Pt for the unmodified sample and ALD alumina modified samples. A similar catalyst without Pt promotion is used as base for ALD Pt modified sample. Around a gram of each catalysts was ran in a micro-reactor from 40 to 70 h. The conversions, selectivity and productivity were quantified to determine the practical qualities of the catalysts. Average crystallite size was determined from XRD to observe possible sintering.

ALD alumina showed the desired effect in reducing average particle size after the run when compared to unmodified catalyst from approx. 20 nm to as low as 14 nm for 40 ALD cycles. As an active component ALD alumina at 5 cycles increased activity and methanation, while at 20 cycles the properties were similar to the unmodified catalyst. ALD Pt coated catalyst showed product selectivity towards lighter products. The hydrogenating effect of platina was strongly present, demonstrating the effectiveness of only 5 ALD Pt cycles. This thesis gave some indication on the effectiveness of ALD modifications for Fischer-Tropsch cobalt catalysts and the synergy between some of the characterization methods used in FTS.

Keywords fischer-tropsch, atomic layer deposition, ald, cobalt catalyst, characterization, top-coating

Foreword

"I may not have gone where I intended to go, but I think I have ended up where I needed to be." – Douglas Adams

I profoundly thank you my dear family, friends, colleagues, mentors and professors. In both life and science, I would not be here if it wasn't for the foundation you have laid in which I today stand.

The cake is a lie,

Patrik Eskelinen

Table of Content

List of Abbreviations

AFM: Atomic Force Microscopy

Al_2O_3: aluminium oxide

ALD: Atomic Layer Deposition

AlN: Aluminium Nitride

ASF: Anderson-Schultz-Flory distribution

BET: Brunauer–Emmett–Teller

BSE: Back Scattered Electrons

BTL: Biomass-to-Liquids

C1-C4: Carbon chain with 1 to 4 carbon atoms

C5+: Carbon chain with 5 or more carbon atoms

Co: Cobalt

Co_3O_4: Tricobalt tetraoxide

CoO: Cobalt monoxide

Cu: Copper

CVD: Chemical Vapour Deposition

EDX/EDS: Energy Dispersive X-ray Spectroscopy

EELS: Electron Energy Loss Spectroscopy

Fe: Iron

FT: Fischer-Tropsch

FTIR: Fourier Transform Infraded Reflectance

FTS: Fischer Tropsch Synthesis

GC: Gas Chromatographer

GTL: Gas-to-Liquids

H_2: Hydrogen

H_2O: water

HfO: Hafnium Oxide

HPLC: High-Performance Liquid Chromatography

HTFT: High Temperature Fischer Tropsch

IWI: Incipient Wetness Impregnation

LTFT: Low Temperature Fischer-Tropsch

MeCpPtMe3: Trimethyl(methylcyclopentadienyl)platinum(IV)

MS: Mass Spectrometer

MTFT: Medium Temperature Fischer-Tropsch

nm: nanometer

ppb: parts-per-billion

R&D: Research and Development

Ru: Ruthenium

RWGS: Reverse Water-Gas Shift

SAED: Selected Area Electron Diffraction

SE: Secondary Electrons

SEM: Scanning Electron Miscroscopy

SIMS: Secondary Ion Mass Spectroscopy

SiO_2: Silicon dioxide

STEM: Scanning Transmission Electron Microscopy

STM: Scanning Tunneling Microscopy

TEM: Transmission Electron Miscroscopy

TiO_2: Titanium dioxide

TMA: Trimethylaluminium

ToF: Time-of-Flight

ToS: Time-on-Stream

TPD: Temperature Programmed Desorption

TPR: Temperature Programmed Reduction

WWII: Second World War

XRD: X-ray Diffraction

XTL: X-to-Liquids

ZnS: Zinc Sulfide

α-Al2O3: alpha aliminium oxide

γ-Al_2O_3: gamma aluminum oxide

Table of Figures

1. Introduction

Fischer-Tropsch synthesis (FTS), named after the inventors of the process Franz Fischer and Hans Tropsch, is a heterogenous catalytic process used to produce hydrocarbons from gas mixtures containing hydrogen (H_2) and carbon monoxide (CO). The catalysts used are mainly iron (Fe), cobalt (Co) and ruthenium (Ru). The process was invented in the early 20th century in Germany and was used to produce fuels very similar to gasoline for ground vehicles. Currently it represents a promising stepping stone to more effectively use available gas sources both fossil and renewable, or to possibly produce petroleum substitutes from industrial sidestreams and captured carbon dioxide (CO_2) converted to CO (see Figure 1 for such a schema). Economically, the motivation for current FTS is to produce fuels where other resources are scarce (i.e.: no crude oil available) or consumption sites are far apart (transport of the precursor gases is expensive).[1]

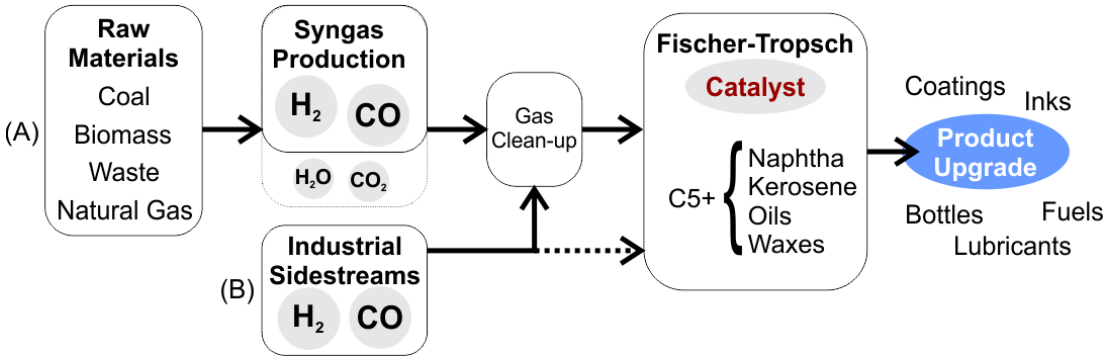

Figure 1. Schematic representation of a process implementing Fischer-Tropsch, from raw materials and alternative sources to products; in syngas production H_2O and CO_2 are possible by-products of the conversion process, while for FTS H_2 and CO are always the primary reactants.

Cobalt-based catalysts are used in FTS to produce hydrocarbon mixtures consisting mostly of paraffins (hydrocarbons chains containing only saturated bonds). The heavier hydrocarbon products can be hydrolyzed into diesel, gasoline or other oil-like products while the lighter products can be distillated and used as is.[1,2] Compared to ruthenium, cobalt is three orders of magnitude more abundant. Compared to iron, cobalt-based catalysts have higher activity and better selectivity towards heavier hydrocarbons. In FTS processes being able to tailor the catalysts for selectivity, activity and resilience is a key factor in enabling more economically attractive

industrial implementations, especially in microtubular reactors were catalyst amounts rarely extends over cubic meter volumes.[1] The previous facts are the motivation for this thesis, which studies cobalt catalysts variations prepared with industrially scalable processes and modified by atomic layer deposition (ALD).

The purpose of this thesis is to compare an impregnated platinum promoted γ-Al_2O_3 supported cobalt catalyst against variations produced on the same support with the addition of ALD top-coating and substitution of the impregnated platinum (Pt) with ALD coated Pt as the promoter (Figure 2). More specifically observing the selectivity and activity of the catalyst are the key metrics in analyzing the success or failure of a catalyst variation. Addition of the top-coating is expected to improve the catalysts long-term stability and resilience to sintering, while addition of ALD Pt is expected to function as the impregnated Pt but with better dispersion despite a lower mass load.

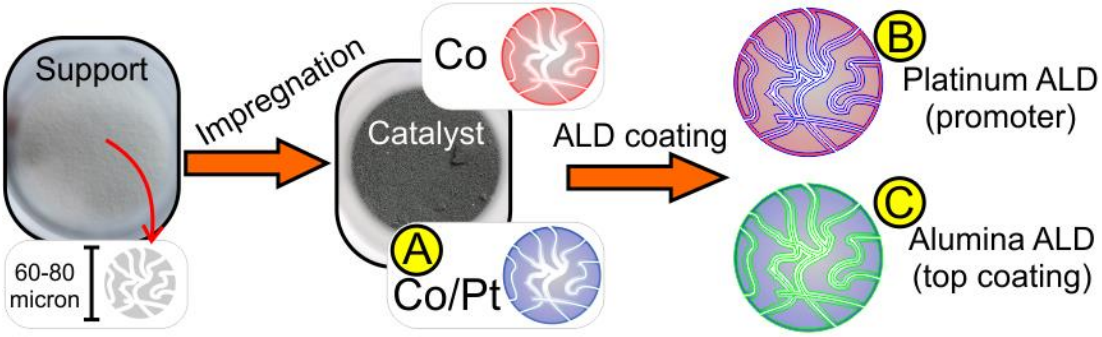

Figure 2. Diagram showing the different catalyst preparation paths for this thesis. Catalysts are prepared into microporous support particles by impregnation and are modified by atomic layer deposition. The catalyst types compared are marked by A, B and C. ALD coatings are illustrated by very thin lines along the pores, while impregnation has a gradient decreasing from the outer shell to the interior of the support particle.

In the following chapters the principles involved in FTS, the nature and production of cobalt catalysts and the involved characterization of such catalysts is presented based on available literature. The biggest portion of this thesis is given to the characterization of catalysts as it is essential and particularly challenging given the physical dimensions in supported catalysts. FTS and accompanying processes have varying levels of complexity, and the literature review hopefully gives enough tools for the reader to understand and reflect on this work.

2. Literature Review

2.1. Fischer-Tropsch Synthesis

Fischer-Tropsch synthesis (FTS) englobes a range of chemical reactions which produce gaseous, liquid and solid hydrocarbons, mainly olefins (hydrocarbon chains containing double bonds) and paraffins (hydrocarbon chains containing only single bonds), from gaseous hydrogen and carbon monoxide. Historically Fischer-Tropsch (FT) processes were developed due to supply shortages and were used to great effect during the pre- and WWII era Germany to produce fuels. Although FT synthesis and processes have been available for several decades the recent interest has been motivated not by shortage, but by environmental factors, integration into current industrial streams and small-scale production. In an age of increasing global temperatures due to carbon emissions, the efficient use of carbon sources is essential. More effective use of both renewable and non-renewable carbon can be targeted and achieved with FTS.[1,3]

The desired range of hydrocarbons from FTS are generally C5+, in particular minimizing the production of C1-C4 are essential for profitability of FT processes. The direct products of FTS are further processed or converted into more valuable products such as polymers, fuels and lubricants; which together with the operative environment have a strong influence on the choice of primary FT products and process conditions. Several industrial schemes are named based on the feedstock and product desired, such as GTL – Gas-to-Liquids, BTL – Biomass-to-Liquids and XTL – X-to-Liquids (X is any source of carbon such as waste). Concerning cobalt catalysed FTS some of the most economically interesting target products are high-viscosity paraffin lubricants and waxes for hydrocracking to produce diesel components.[1,2] A few of the side products formed are alcohols and even aromatic compounds in minute amounts.[1,4]

FTS is a catalytically activated process with essentially three different catalyst options; iron, cobalt and ruthenium. Where the former two are employed industrially, the rarity and high-activity of the latter finds its use in research only. As

can be inferred, FTS cannot be described by a single chemical reaction, or even a single pathway of chemical reactions.[1,2] Table 1 summarizes the reactions involved in FTS. The reactions are mostly exothermic, and the released energy can be used to drive the process or for energy conversion. Several reaction mechanisms have been proposed, their particulars debated and further validated in multiple instances, inferring FTS consists of multiple reaction mechanisms acting in tandem.[1] The specific reaction pathways are still under investigation, i.e.: even though iron catalysts are found as carbides while ruthenium and cobalt catalysts are used in metallic state both produce similar main products. The varying side products from the different catalysts show the complexity of the process.[1,2,4,5]

Table 1. Overall main postulated reactions involved in Fischer-Tropsch synthesis.[1,6]

Main Fischer-Tropsch related reactions:	
Paraffin synthesis	$(2n+1)\mathrm{H_2} + n\mathrm{CO} \rightarrow \mathrm{C}_n\mathrm{H}_{2n+2} + n\mathrm{H_2O}$
Olefin synthesis	$2n\mathrm{H_2} + n\mathrm{CO} \rightarrow \mathrm{C}_n\mathrm{H}_{2n} + n\mathrm{H_2O}$
Water gas shift reaction	$\mathrm{CO} + \mathrm{H_2} \rightleftarrows \mathrm{CO_2} + \mathrm{H_2O}$
Alcohol synthesis	$2n\mathrm{H_2} + n\mathrm{CO} \rightarrow \mathrm{C}_n\mathrm{H}_{2n+1}\mathrm{OH} + (n-1)\mathrm{H_2O}$
Boudouard reaction	$2\mathrm{CO} \rightleftarrows \mathrm{C} + \mathrm{CO_2}$
a. Catalyst reduction/oxidation	$\mathrm{M}_x\mathrm{O}_y + y\mathrm{H_2} \rightleftarrows y\mathrm{H_2O} + x\mathrm{M}$
b. Catalyst reduction/oxidation	$\mathrm{M}_x\mathrm{O}_y + y\mathrm{CO} \rightleftarrows y\mathrm{CO_2} + x\mathrm{M}$
Bulk carbide formation	$y\mathrm{C} + \mathrm{xM} \rightleftarrows \mathrm{M}_x\mathrm{C}_y$

The reactant gases in FTS are H_2 and CO, these reactants originate from a gasification or similar gas conversion process, and the product of such processes is named syngas. Syngas from different feedstock (biomass, waste, coal or natural gas) have different stoichiometry of H_2 and CO, besides having CO_2, N_2, water and harmful impurities such as sulphur compounds. FT processes are essentially designed for a certain syngas and attention is reserved for gas clean-up to avoid poisoning the catalysts. A typical catalyst poison especially troublesome for cobalt is H_2S which has a process limit in the parts per billion (ppb) range. Thus before feeding syngas to a FT reactor the gas is typically washed, passed through an activated carbon bed and a guard bed.[1]

A consequence of the FTS reaction mechanism is that the reactor, catalyst, target product and the feedstock all play a crucial role in the overall productivity, efficiency

and throughput in industrial implementations. After selection of the target product (a specified range of hydrocarbons) several of the tuneable parameters are process engineering issues, such as reactor type, heat transfer, recovery processes and further downstream processes; all of which hinge on the properties of the catalyst in use.[1,4] Overall catalyst development accounts for the majority of R&D involved in FT processes in number of publications, as shown by the simple search result hits presented in Figure 3.

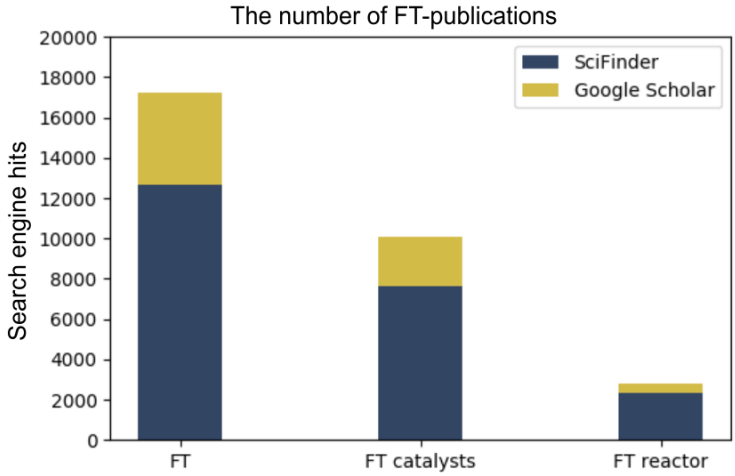

Figure 3. The number of publications in Fischer-Tropsch by topic found in SciFinder and Google Scholar from the years 2010 until 2018.

The FT chemical reactions are mediated by surface sites and surface chemisorpted species which react step-wise. The step-wise reaction is a type of polymerization reaction which results in the Anderson-Schultz-Flory (ASF) product distribution. The ASF distribution is defined by an empirical alpha factor indicating chain growth probability.[1,4] Even though the surface reactions are uncontested the particular locality and atom transfer mechanisms are still under debate. The most accepted pathways of reaction are the associative and the dissociative pathways.[1] This work focuses on cobalt catalysts and a more detailed and focused description of the reaction mechanism involved is provided in the next section. In summary, and with severe simplification, the associative pathway involves insertion of CO into the chain growth and elimination of the oxygen atom by hydrogen from the chain. The dissociative pathway involves the dissociation of CO to the surface forming carbene {C} and adsorbed atomic oxygen {O}, the reaction of {C} and adsorbed hydrogen {H}

forms hydrogen containing species {CH_n}, which can associate at sites for chain propagation until terminated to R-CH_3.[4,7,8]

Given the important role of temperature in FTS there are a few practical ranges defined in FT processes. Low temperature Fischer-Tropsch – LTFT (<250 °C), medium temperature Fischer-Tropsch – MTFT (250-320 °C) and high temperature Fischer-Tropsch – HTFT (> 320 °C).[1–3] In LTFT heavier hydrocarbons are produced, while in HTFT only iron catalysts can be used due to methane selectivity for cobalt. HTFT also produces high grade steam which can be used for energy conversion, and higher activity as well as higher single pass conversions are possible. On the other hand, driving the reaction at high temperatures leads to faster deactivation. Thus, typically, cobalt is used exclusively in LTFT temperature ranges.[1,9,10] It is well understood that at lower temperatures desorption events are less likely which increases the fraction of heavier products in FTS, due to this, investments in FT processes are typically focused on LTFT and MTFT applications.[1,4]

2.2. Fischer-Tropsch cobalt catalysts

Cobalt-based catalysts are one of two catalysts types used for FTS industrially, the other being iron-based catalysts. The reason is purely economic because even though ruthenium has the highest activity among FT catalysts it is a very rare and consequentially expensive metal. Cobalt is significantly costlier than iron-based catalysts, but cobalt catalysts are typically supported, the catalytic activity is high at low-temperatures and the product range is more selective towards heavier hydrocarbons. Also the lifetime of cobalt-based catalysts extends for years such that it offsets the economic advantage of iron in specific use-cases.[1] The product range of cobalt-based catalysts is remarkably different from that of iron-based catalysts, among other factors: cobalt catalysed FTS is not reverse water gas shift (RWGS) active, so it cannot produce CO and H_2 from H_2O and CO_2; cobalt-based FTS produces a very minor amount of oxygenated products (< 1 wt%) as compared to iron-based FTS (~ 5 wt%); FTS using cobalt-based catalysts also favour longer hydrocarbons since they operate in LTFT regimes as opposed to iron-based FTS which operate in MTFT or HTFT.[1,11] In addition to the selected metal, catalytic activity can also be tuned by the addition of promoters such as platinum, nickel or copper.[1,12,13]

A freshly produced cobalt catalyst contains cobalt oxide (Co_3O_4 or CoO) but cobalt must be in metallic form for the surface reactions to take place, thus reduction is a critical step in the catalyst preparation. Catalyst reduction takes place by flowing pure hydrogen, or a mixture of hydrogen and inert gas, over the catalyst at high temperatures. The temperature for reduction of cobalt catalysts range from 300 to 500 °C. Lower temperatures are preferred since they defer the formation of secondary phases such as aluminates, or silicates, but the main criteria for selecting temperature is defined by the reducibility of the catalyst. After reduction the catalyst matrix loses mass and the final morphology of the catalyst is formed. The exact nature of an FT-catalyst is actually characterized from the reduced form of the catalyst.[12,14,15]

The size of cobalt particles or crystallites is ideally ≥ 8 nm in diameter which balances the stability and surface sites for FTS conditions. The atomic surface of such cobalt particles can be described by terraces, edges, corners and kinks, see Figure 4 below. The chain growth reactions have been shown to take place primarily on kinks, edges and corners as the coordination number of these sites is lower and there are more possibilities for bonding.[1,11,16] Cobalt-based catalysts are typically produced by impregnation into a support or by co-precipitation with a support. Supports being compounds which provide the mechanical stability and surface for the high dispersion of the catalyst. Typical supporting materials are refractory in nature such as particles of aluminium oxide or titanium oxide.[1,12,13]

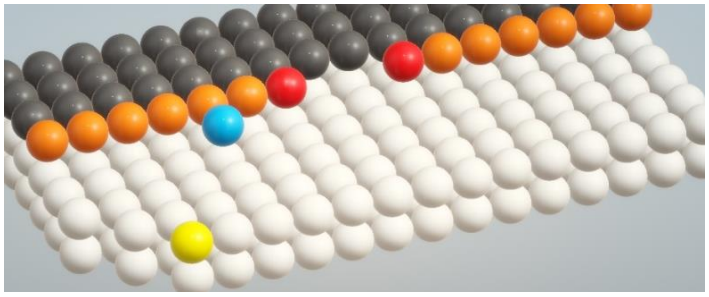

Figure 4. A ball model representing surface features at the atomic scale in a crystallite. Each ball represents an arbitrary atom X; colours define a feature: yellow = single corner atom, blue = step adatom, orange = step atoms, red = kink atom, grey = terrace.

The main products in cobalt FTS are paraffins, olefins and a very small fraction of cyclic compounds or alcohols. Cobalt is limited to low temperature regimes for a few reasons, it is a strongly hydrogenating catalyst which produces more methane as the temperature increases and the stability of the catalyst at higher temperatures is poor. The two pathways associated with FTS are the associative and dissociative pathway, and although both have merits, the dissociative pathway is better proven by evidence.[1,17,18]

Using the dissociative pathway and cobalt catalysts as the framework to explain the FT reactions, it is found that FTS depends on certain surface reaction sites. The activation of H_2 into {H} is very well understood in metal surfaces and occurs promptly, and the adsorption of CO and cleavage into {C} + {O} on a metal surface is also well accepted and supported. The formation of $\{CH_n\}$ species occurs by the

diffusion and bonding of {H} with {C} in the metal surface, but there is no chain growth in planar defect-free close-packed surfaces; in such a surface only methane is produced. When steps and kinks are present in larger metallic particles, dissociation of {CO} into {C} and {O} is facilitated and chain propagation can take places at the open corners by addition of {C} or {CH_n}.[16,17,19] This pathway is strongly corroborated by quantum chemical computations which are independent of rate limiting assumptions.[19]

2.2.1. Preparation of Fischer-Tropsch cobalt catalysts

For FT cobalt catalyst preparation few methods are used widely on an industrial level. Considering cobalt's availability and cost, it is only prepared supported, the supporting materials are typically alumina (Al_2O_3), silica (SiO_2) or titania (TiO_2) based with high surface area and porosity. The preparation methods specifically target maximal surface area and particle size consistent with features desirable for FTS, which are maximal concentration of edges, kinks, corners and steps at the atomic scale, and high dispersion and uniform distribution of cobalt at the particle scale. Careful consideration is given to the support which may interact strongly with the metallic catalyst, such interaction is mediated by the phase, additives and even acidity.[1,15,20] The preparation methods used industrially are by a large-majority based on impregnation of catalyst salts into the support[21] or co-precipitation of catalyst metal and supporting matrix[22], as showed schematically in Figure 5.

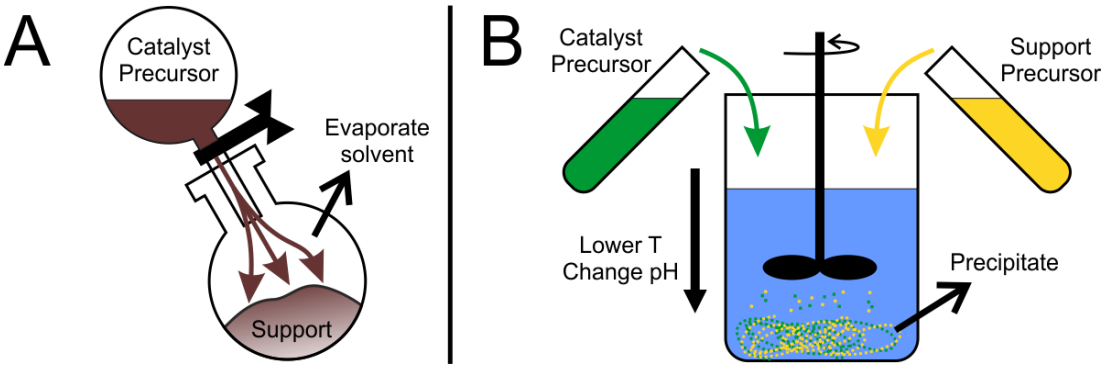

*Figure 5. Schema of the catalyst preparation by impregnation (**A**) and co-precipitation (**B**). **A:** Catalyst precursor is added to the catalyst support by vacuum, immersion or other method; end product is calcinated. **B:** Catalyst and support precursors are mixed and both support and catalyst precipitates from supersaturated solution.*

Impregnation methods produce the oxide form of the metals and thus before actually using the catalysts a reduction step is performed.[1] The addition of promoters can be realized by impregnation or a more novel approach is to use thin film deposition techniques, such as atomic layer deposition (ALD) which provide high dispersion and uniformity[23–25]. An issue with catalyst preparation is that small variations in each step add-up affecting significantly the properties at the nanoscale in which rigorous descriptions would be relevant, making it difficult to correlate qualitative factors with products from actual FT processes.[1,26]

Impregnation

A simple method used in preparing supported FT catalysts is impregnation, in which a liquid carrier containing the intended deposition material is contacted with the supporting solid. The liquid carriers are salts of the deposition metal, such as cobalt nitrate. There are several impregnation processes with different details on mass-transport, adsorption and surface exchanges.[21] The impregnation can be affected by the pH, type of solvent and concentration on the liquid carrier, while texture, surface functional groups and reactivity affect the solid support. The interactions between the carrier and support have to be considered during preparation.[4,13] A variation typically used is dry impregnation, or incipient wet impregnation (IWI), in which the volume of liquid does not exceed the volume of the pores in the substrate, leading to a uniform distribution. Variations of IWI such as using a supersaturated solution of the salt leads to non-uniform distributions, in this case an eggshell distribution where a thin crust of the catalyst salt is formed on the surface of the support particle.[1,13,21] In case of wet impregnation the drying of the carrier liquid, typically water, can be performed under heat, vacuum and stirring conditions, which affect the distribution of the catalyst salt.[1]

Atomic Layer Deposition

Atomic layer deposition (ALD) is a thin film deposition method by which cyclic complementary reactions allow the growth of almost atomically conformal layers.

The method can be identified as a sub-type of chemical vapour deposition (CVD) as it relies on chemical reactions from gaseous sources to drive the growth process. ALD excels particularly in the growth of very thin conformal films of a wide-range of substances (i.e.: Al_2O_3, AlN, ZnS, HfO, etc…), on a wide-range of materials (silicon, metals, ceramics). At the extreme end of the spectrum conformality of ALD is shown in Figure 4, where ALD achieves reasonably conformal growth in nano-scale trenches.[27,28]

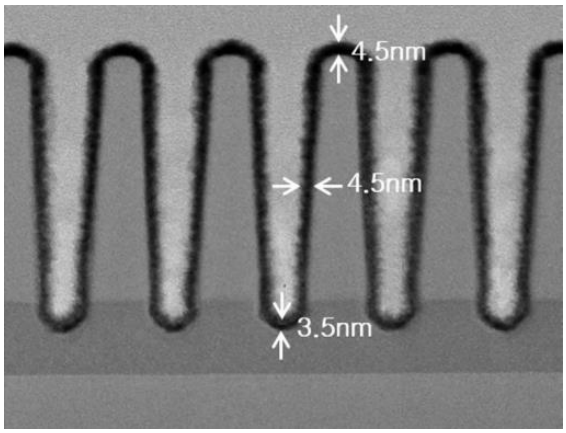

Figure 6. An example of a nanostructure coated with extremely conformal ALD film. XTEM image of the ultrathin ALD-Mo2N films coated onto the nano-scale trench structures. Retrieved from Jang et al.[29]

Essentially the deposition consists of four phases: a pulse of precursor gas is introduced which reacts with the surface until surface coverage is achieved; when the over-provisioned precursor cannot react further, inert gas is introduced and the chamber is purged; now a pulse of the complementary precursor gas is introduced which reacts with the surface formed on the first pulse, restoring it to the initial state; a final inert gas pulse is introduced and the chamber is purged. These cycles are repeated for specific thicknesses, the mechanism is illustrated in Figure 7. The growth mechanism of ALD does not necessarily generate a complete atomic layer per cycle, precursor molecules maybe larger than the target deposition group and 2-3 cycles might be required per atomic layer. The growth per cycle depends largely on the process but typically around 1 Å.[27,30]

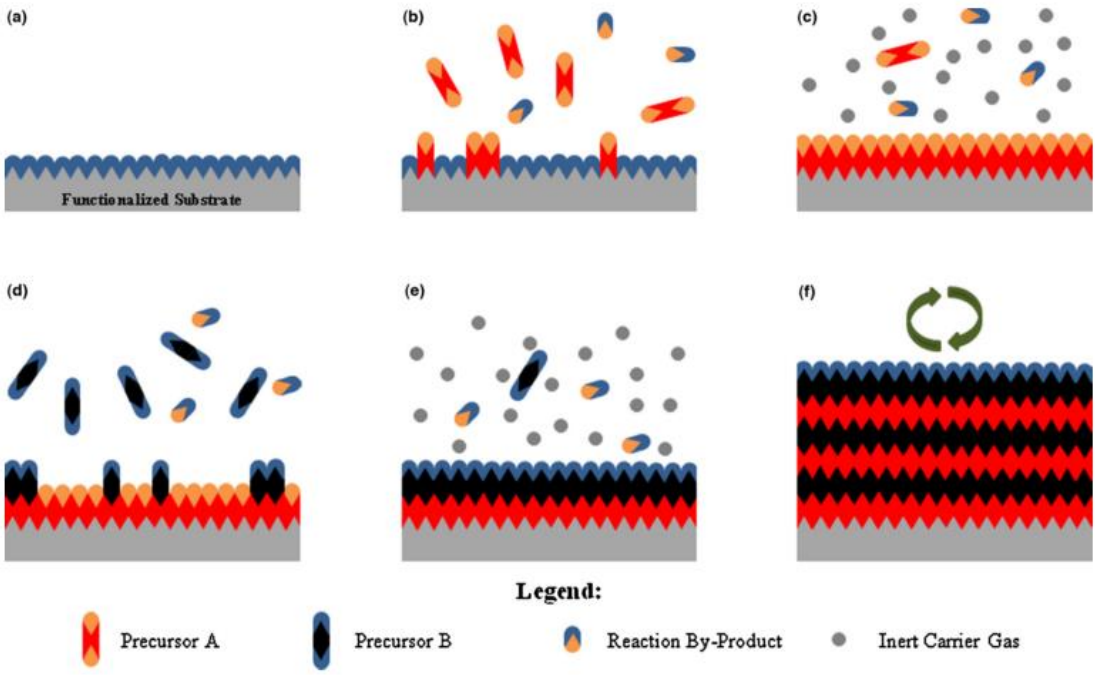

Figure 7. Schematic figure showing the step-wise growth of films by ALD; (a) a surface with functional species; (b) pulse of precursor and surface reaction; (c) achieving surface saturation and purging; (d) pulse of second precursor and surface reaction; (e) surface saturation, initial functional surface characteristics are restored, and purging; (f) repeat previous steps for film growth. Retrieved from R. W. Johnson, A. Hultqvist, and S. F. Bent (2014).[27]

Relevant for the application of ALD are the deposition conditions used. Because of the growth mode used, temperature and pulse times are critical parameters for the formation of a monolayer on the available surface. Chemisorpted species (covalent bonds formed) can migrate on the surface or degrade at high temperatures. At low temperatures the reaction kinetics are unfavourable and precursor gases may condensate. These limit the reactor temperatures of specific ALD processes to a range referred to as the "ALD window", typically this range is below 350 °C and the span can be as low as 10 °C or even as high as 100 °C.[27,30] The different deposition regimes are shown in Figure 5. Process optimization is of major importance when using expensive precursors. Ideally injection of precursor gas is as close as possible to the needed mass for fully saturating the surface, and in practice some over-provision is needed. The overprovisioned precursor is in turn purged with the inert gases leading to waste. Pulse times in commercial ALD equipment can be on the order of tenths of seconds. On the other hand under-saturation is also possible if pulse times are short or the substrate has very complex and large aspect ratios.[27,28]

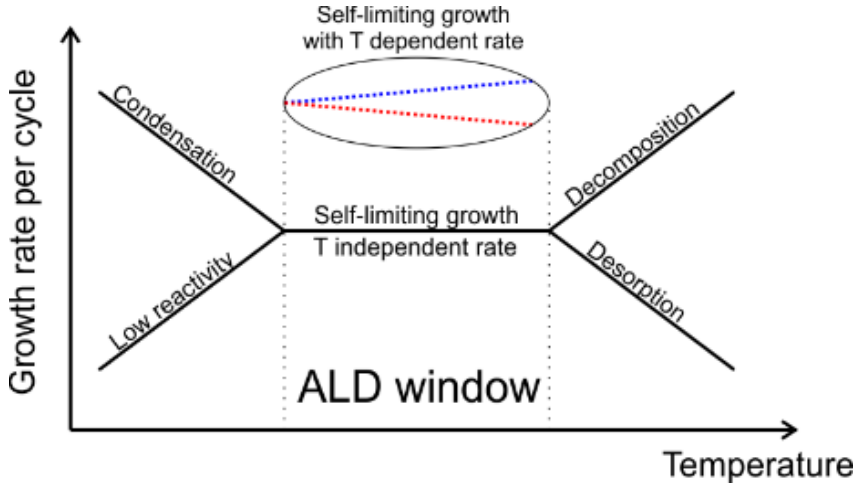

Figure 8. Schematic figure showing the different growth regimes possible in a generic deposition setup. Strictly ALD only occurs within the ALD window when surface saturation is achieved, and growth is not time-dependent. Different materials might also show a mild temperature (T) dependent rate (dotted blue and red lines) within the ALD window. This dependence can be both positive (i.e.: for Pt ALD) and negative (i.e.: for AlO ALD).[31–33]

A different issue especially relevant to ALD are the growth patterns which can be achieved with the process. Several noble metals will preferably nucleate and coalesce into islands before forming a uniform layer, a configuration which minimizes their high surface energy,[34] while oxides will typically form smooth layers.[32] These limitations originate from the thermodynamics of the system. A prototypical deposition process for a smooth oxide is achieved through ALD deposited Al_2O_3. The precursors for such deposition are trimethylaluminium (TMA) and H_2O, which has a wide ALD window from 30 to 325 °C.[27,35] The growth of the noble metal platinum from the precursors Trimethyl(methylcyclopentadienyl)-platinum(IV) (MeCpPtMe3) and oxygen follows a growth regime called Volmer-Weber in which islands of the noble metal are formed. After a critical thickness there is sufficient coverage and islands coalesce into a single sheet and growth follows a layer-by-layer pattern.[36] The ALD window for the Pt process using MeCpPtMe3 extends from 250 to 300 °C.[33] This growth pattern has obvious implications for the use of certain ALD deposition processes when very low layer thicknesses are targeted, i.e.: formation of nanoparticles and clustering instead of a thin-layer.

Modification by atomic layer deposition

The diverse deposition materials afforded by ALD, over a 1000, may give a substantially more effective means of adding materials to the catalyst surface in a specific order and with tight constraints.[24] In particular the application of protective layers against sintering and poisons have been shown to produce more resilient catalysts without compromising productivity.[23–26] Porous catalyst support can be considered extremely high aspect ratio structures which are difficult to access, yet the uniform growth of intra-porous additive layers is desirable for the modification of catalysts. ALD has been used to modify catalysts by applying s and promoters successfully.[24]

The coating and addition of promoters (0) by ALD into cobalt catalysts is a particularly difficult tasks, mainly due to the gas diffusion of precursor gases into the porous structure. Modelling work describing deposition of high aspect ratio systems in electronic devices have a longer history, but the order in such systems is not comparable to the porous nature of catalysts supports.[37,38] ALD deposition in such porous structures require more general models which can account for surface area, pore diameter and mass balances with appropriate dose-times at specific pressure. The model presented in the work of Elam & Yanguas-Gil estimates the required increments to dose-times based on diffusion and surface reaction probability in nanostructures. The additional dose time increments are presented in Figure 9.[38]

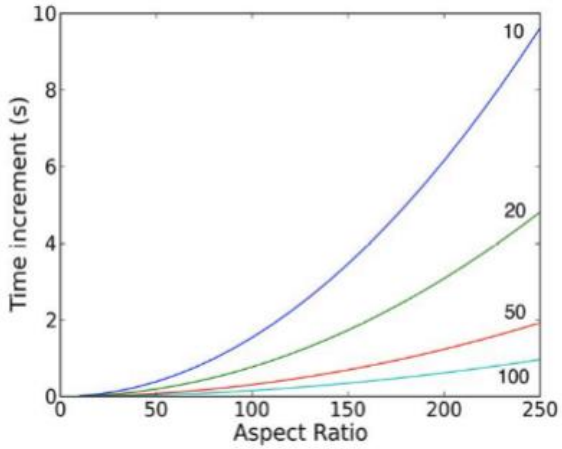

Figure 9. Time increments necessary to achieve surface saturation for a given process at a certain precursor partial pressure (10-100 Pa, lines of different color). Retrieved from Elam & Yanguas-Gil.[38]

There is a clear incentive to apply rare materials such as platinum and iridium (stabilizing and alloying) elements by ALD compared to traditional methods because of its precise loading and penetration depth. While ALD top-coating of i.e.: alumina is incentivized by the digitally controlled thickness even in microporous substrates.[24]

2.2.2. Properties of Fischer-Tropsch cobalt catalysts

Properties relevant for supported FT cobalt catalysts are morphology, selectivity, activity, deactivation and promoters and implied composition; each of these can be characterized for cobalt catalysts by a multitude of methods and affect performance distinctively.[1,13] Morphology describes the physical shape and form of the catalyst, which mostly affects physical phenomena such as mass, heat transfer and surface area. However, morphology also determines to an extent crystal domains which affect strain and furthermore the surface chemistry.[39] The selectivity describes the product distribution of the FT-process with a given catalysts and indirectly points to the underlying reaction mechanism.[1,40] Activity and deactivation are defined by the amount of product generated and the negative trend in respect to time, having a significant weight in the economic viability of a catalyst.[1,5,10,41] The addition of promoters is an important quality of a catalyst, and discussion on catalyst formulation is limited to the addition of promoters and top-coating, although catalyst support plays just as important a role.[1,15] The following sub-sections discuss each separately.

Morphology

Morphology concerns the physical shape and form of the catalyst, relevant for the mechanical behaviour and mass transfer of an FTS system. Morphology also has implications for the crystal strain of the active metal and reactor selection. Where supported catalysts are concerned, the morphology is primarily described by the support. In low metal loadings the metallic layer formed is thin, and the structure retains the porosity and overall shape of the support. In high loadings, formation of an egg-shell type structures is possible.[14] At the nanoscale the diameter and volume of the pores and the specific surface area all have great influence on the catalyst

performance. Typical pore volumes are on the order of < 1 cm3/g and pore diameters *d* vary from very small pores with *d* < 7 nm to large pores d > 12 nm. These values originate from the support formulation, supports based on alumina have several phases with γ-Al_2O_3 having typically the largest surface area and smallest pores while α-Al_2O_3 has lower surface area and larger pores.[12,39,42] For perspective, maximizing surface area has limits for FT catalysts, larger surface area and smaller pores are associated with higher tendency to deactivate, possibly due to trapped condensed water and increased strain on cobalt crystallites.[5,39]

Selectivity

The mechanism of FTS defines the range of hydrocarbons which can be produced and the final product fractions. It is not possible to obtain a single hydrocarbon chain length from FTS because of the statistical nature of desorption events and step-wise chain growth. It is useful to define selectivity as a minimization of side products such as oxygenates and the peak fraction with a specified range of chain length. For specific applications chain length fractions of different sizes can be more useful. In some scenarios C12-17 can be more useful than <C12 or >C17 and in this context tailoring a catalyst and process for this range, with minimal side-products, is valid concept for selectivity.[1] The FTS product range is described typically by the Anderson-Schultz-Flory (ASF) distribution shown in equation (1) below with a few product distributions shown in Figure 10, where W_N is the weight fraction for a carbon chain of length *N* and α is the chain growth probability factor:

$$W_N = (1-\alpha)^2 \times \alpha^{N-1} \quad (1)$$

By observing even a slice of the product distribution it is possible to calculate the α value of the process.

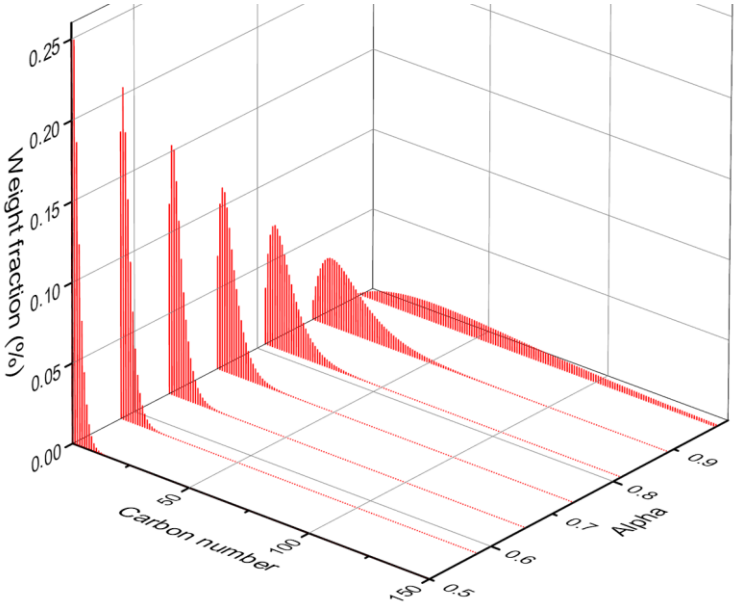

Figure 10. Weight fractions generated from different α values applied to the Anderson-Schultz-Flory distribution as given in equation 1, lower α values give lighter products (closer to carbon number edge), while higher α values produce heavier fractions (opposite end of carbon number edge).

The main factor affecting the product selectivity is temperature. At lower temperatures heavier fractions are expected and at a higher temperature boundary only methane is formed. Pressure also affects selectivity analogously to temperature. The previous leads to a trade-off were productivity must be balanced at expense of selectivity towards higher carbon numbers, as increasing temperature leads to a lighter product. Several approaches have been used to tune the selectivity of catalysts, such as, use of promoters, production of catalysts with very specific morphologies and tuning of the process parameters. There are intrinsic limitations to selectivity which are purely due to the polymerization reactions.[1,3,18]

Activity and Deactivation

Catalyst activity is described by the productivity of a catalyst as related to the amount of catalyst and temperature of the process. The more active a catalyst is, the more product is obtained per gram catalyst at a specified temperature and mass-transfer, which is related to productivity parameters.[1,13] The activity as a function of time of FT cobalt catalysts is crudely represented in Figure 11. Catalyst activity is initially very high, with a sharp drop until a stable configuration is achieved. Catalysts formulations

might fall into multiple steady-states in which the system might seem to be at equilibrium, although the initial high activity has not been stabilized.[1]

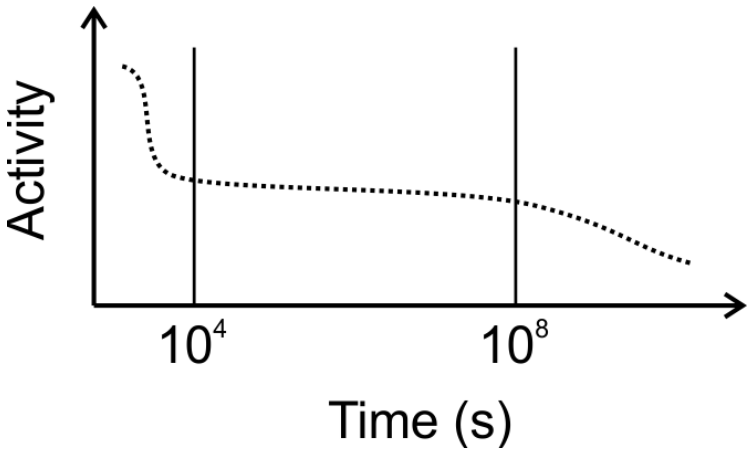

Figure 11. Representative activity of a typical FT cobalt catalyst as a function of time. Initial activity is very high but decays in hours; normal operation lasts years without significant decay in activity; finally catalyst activity starts decaying more rapidly and the catalyst is spent.[1]

The overall productivity of a catalyst and process is tied to the useful lifetime of the catalyst and its activity. In FT reaction conditions all catalysts will eventually deactivate due to several different reasons which can only partially be mitigated by increasing catalyst complexity and engineering effort. Factors leading to deactivation include attrition and crushing, especially when the catalyst bed is not fixed, thermal degradation such as sintering, poisoning by contaminants such as sulphur, fouling by formation of carbonates or coke on the catalyst surface, volatile carbonyl formation by carbon monoxide, reactions between catalyst metal and support, and oxidative reactions by excessive water or carbon dioxide.[1,10,13]

Catalyst deactivation has two obvious criteria for identification; either the productivity of the catalyst drops or selectivity changes unfavourably under the same conditions compared to a previous point in time.[13] Cobalt-based FT catalysts tend to be significantly more stable than iron-based catalysts with cobalt catalysts being operated industrially even up to 5 years.[1,4] Besides poisoning, the most severe deactivation processes are surface oxidation, which eliminates active surface sites, and sintering which lowers overall surface area. In particular cobalt catalysts are an order of magnitude more susceptible to sulphur poisoning than iron catalysts.

Commercial operation of cobalt catalysed FTS require sulphur concentrations below 4 ppb on the incoming stream.[1]

Two pathways for the water-assisted oxidation of metallic cobalt are apparent: the direct oxidation of cobalt by water ($Co + H_2O \rightarrow CoO + 2\{H\}$), and the oxidation of surface cobalt by surface dissociated oxygen atoms from CO ($CO \rightarrow \{C\} + \{O\}$; $Co + \{O\} \rightarrow CoO$). In the latter, abundance of water in the environment inhibits the release of surface oxygen which in turn can react to form oxides ($CO \rightarrow \{C\} + \{O\}$; $\{O\} + H_2 \rightarrow H_2O$), this second pathway also seems to be dominant in the formation of CoO in high conversion FTS due to excessive water formation.[7,43] Under direct influence of water a film of hydroxyl groups is formed on the cobalt surface, which has been shown to be stable.[7,44] This is supported even when considering the surface energy of nanoparticles.[43] Direct evidence of oxidation in cobalt nanoparticles has been shown,[45] but the extent of this oxidation is not well defined, it is clear that smaller nanoparticles < 4 nm are readily oxidized, while larger nanoparticles > 8 nm under high conversion conditions may be subject to long-term deactivation by surface oxidation. Literature also suggests an increase in nanoparticle sizes at higher temperatures due to sintering in normal operation, which is a slow process. However, during the activation phase of a catalyst sintering was shown to be very sharp for particles smaller than < 8 nm.[9,43,45–48]

Promoters

Additives for catalysts, generally named promoters, are any active element added to the main catalytic metal to improve activity, selectivity or another property of the catalyst for its operation. The use of promoters is prevalent in current FT catalyst development to essentially tune the selectivity and improve the economic viability of different implementations. As a general example, iron-based FT catalysts require alkali metal promoters to adjust the acidity of the catalyst surface, and other additives such as Cu to assist in the reduction of the catalyst. In cobalt-based catalysts promoters serve several complex functions, such as assisting in the reduction of the starting cobalt oxide, and in stabilizing the dispersion of the cobalt crystallites. Both

are important due to the dynamic state of the catalyst surface during FT reactions.[1,5,12] Elements used as promoters in cobalt FT catalysts include metals from the Groups 9-11 which associate and form alloys with cobalt. For instance, the use of platinum has been shown to assist in both the reduction and dispersion of cobalt within the catalyst body. Other promoters used might affect the physical structure of the catalyst and include Al_2O_3 or Zirconia, which can affect the function of the catalyst by affecting crystal strain or surface re-structuring during reduction and the FT-process.[1,5,39]

2.2.3. Characterization of Fischer-Tropsch cobalt catalysts

Given all the factors presented in previous sections, it is not surprising that catalysts characterization is a very complex and arduous task. As with many heterogeneously catalysed processes, for FT catalysts the time domain of the reactions span femtoseconds while the thermodynamics of the process span hours. Factors characterized include at the macro-scale: reactor design, heat-transfer and mass-transfer; while at the atomic scale: chemisorption and surface reactions.[1,4] A swath of different characterization methods have been applied to FT catalysts targeting all its different aspects; including surface morphology, composition, phase, active-area, activity, deactivation and particle size, among others.[1,13,18,20,49] Because of its complexity several characterization methods will be presented, and the use of at least a few of these methods can be employed to differentiate a productive catalyst from a non-productive. While the previous is sufficient, understanding and relating features in different scales decreases the need for trial-and-error in catalyst development significantly.[13,20]

Microscopy

Given the dimensions of FT cobalt catalysts the use of microscopy is essential for thorough characterization. There a several approaches to microscopy many of which are useful in FT-catalyst characterization. Appreciable magnification and

characterization can be achieved by both scanning and transmission electron microscopy (SEM, TEM), scanning tunnelling microscopy (STM), and atomic force microscopy (AFM), all of which have been employed in analysis of FT-catalysts[11,13,20,24,49–51]. Computationally augmented optical methods such as profilometry can be used for support particle sizing, nevertheless optical microscopy methods are barely employed in current FT catalyst investigations, as magnification is too limited.[13]

SEM is a common and widely accessible characterization method. A beam of accelerated electrons is scanned through the sample surface and the resulting interaction of the beam and sample generates a myriad of responses which are sensed. The response signal can originate from back-scattered electrons (BSE) or secondary electrons (SE) for imaging, and many SEMs and TEMs are equipped with energy dispersive X-ray spectroscopy (EDX, EDS) detectors for elemental mapping (discussed further in spectroscopy).[51] Each of these electron types are useful for different purposes and understanding the modus-operando of each assists in interpreting even the simplest of micrographs.

Since the image on a SEM is formed by scanning a material line-by-line a key concept in the final projection is the interaction volume of the beam at each location. The emission depth of a BSE is much deeper than that of a SE and is inversely proportional to the atomic number of the elements on the beam, giving contrast based on compositional information. Topographic information is significantly harder to observe at smaller scales because the interaction volume can be very large typically < 1 micron at 15 kV. SE electrons are emitted close to the surface of the sample with energies < 50 eV, and their interaction volume is comparable to the size of the beam, allowing even sub-nanometre lateral resolution for edges. The formation of a SE depends also on composition, but contrast is mainly due to edges where more electrons can be emitted compared to flat surfaces.[50,51]

SEM can be used to characterize the surface morphology, rough (> 1-micron resolution) cross-sectional catalytic composition, and, in a few scenarios, to

determine the size of nanoparticles of FT cobalt catalysts. With SEM, scanning a significant portion of a catalyst sample is feasible and the variance on the composition and morphology of cobalt catalyst particles (supported or otherwise) can be observed. This may be relevant for tuning the production schemes of catalysts to obtain uniform results with predictable outcomes. TEM can resolve atoms in crystalline structures and is especially useful to determine precisely the size and structure of nanoparticles and crystallites in FT cobalt catalysts. Coupled with the EELS and electron diffraction the specific composition of nano-crystallites and interfaces can be determined with nanometre lateral resolution. The significant limitation of TEM is that samples are typically only tiny particles or sections thinner than 100 nm. With generally high preparation demands it becomes very difficult to ensure that the TEM sample is representative of the macroscopic sample and not an artefact of the preparation method.[13,20,50,51]

In TEM the image is formed by the electrons being transmitted through a sample hitting a detector. The detector can capture the whole field at once, typical in a TEM, or in a scanning geometry which allows higher resolutions (STEM). The image generated is in all cases a projection of the object through which the beam is transmitted, which has significant implications for the interpretation of the image. Contrast in TEM is generated by phase-shift, transmittance, scattering factors, and electronic properties of the material in the beam path. The transmission geometry permits besides EDS analysis, also electron energy loss spectroscopy (EELS) analysis of the sample (discussed further in spectroscopy). TEM is also capable of diffraction at nanometre scale, probing the crystalline structure of single crystals or nanoparticles (discussed further in diffraction).[50,51]

Spectroscopy

The usage of spectroscopic methods for the characterization of FT-catalysts is nuanced and challenging. Most spectroscopic methods, such as FTIR and Raman spectroscopy, benefit from in-situ configuration to observe the surface products of FTS during the process, because their spectra frequency range probes functional

groups (-OH, -CO, -COH, etc.). While many other spectroscopic methods can probe only the very surface of the catalyst support, or might be otherwise limited by their resolution.[20,51,52]

Energy dispersive X-ray spectroscopy (EDS or EDX) and electron energy loss spectroscopy (EELS), which are found in conjunction with electron microscopy systems, are widely used characterization tools for microscopic materials. In EDS the highly accelerated electrons of electron beam (at the very minimum 5 kV) interact with the atoms on the beam path ejecting a ground-state electron from its orbital creating an electron-hole. An electron from an upper shell drops from its orbital to fill the electron-hole vacancy by emission of a characteristic photon in the process. The photon energy and counts are measured by an energy-dispersive spectrometer. The uniqueness in the electronic structure of each element allows the quantification of the elements present in the probed area. The limitation in resolution from EDS is due to the electron probe interaction volume. Emission photons may be generated from the same volume which generates BSEs and, for a 15 kV acceleration voltage, is on the order of 1 micron in a SEM. In a TEM, EELS is possible due to the transmission geometry and probing energies. Electrons passing through the sample may suffer inelastic scattering, thus losing some energy. The energy spectra of the transmitted electrons are quantified in an electron spectrometer. This energy-loss can originate from different interactions, such as plasmon excitations, phonons, Cherenkov radiation and electron energy-band transitions. This gives EELS better qualitative capabilities than EDS, at least up to the transition metals, and affords for instance determination of oxidation state and different allotropes. The resolution of both EDS and EELS in a TEM are essentially limited by the probe size, and can achieve atomic resolution (in TEM), although electron scattering effects are difficult to overcome.[50,51,53]

The use of spectroscopy in within electron microscopes allows for a very localized characterization of the catalysts, which can be fundamental for understanding the nanoscale phenomena ubiquitous in FT-catalysts. The degree of reduction,

segregation of material phases, distribution of elements, including contaminants and promoters are all examples of properties which can be directly characterized with EDS and EELS.[49–51,53]

Diffraction and scattering methods

Diffraction methods include powder X-ray diffraction (XRD) for phase identification semi-quantitatively, and selected area electron diffraction (SAED) in electron microscopy instruments for phase identification within nanostructures. Both include a powerful collection of tools to determine and support findings in the bulk scale as well as the microscopic scale.[50,54] XRD in particular has been used in recent publications to support claims of homogeneity, purity and crystallite size in FT catalysts,[12,25,41,55] while electron diffraction was used to examine the crystalline phase of nanoparticles.[25,56]

The principle of diffraction is the wave-like interaction of photons or electrons with a material causing reflections, or scattering, and interfering constructively or destructively to form a regular pattern of dark and light areas. This phenomena in a real crystal is named Bragg diffraction. With a specific and narrow source wavelength the diffraction pattern provides information on the interspatial distance between reflection planes using Bragg's law (equation (2)) where *d* is the distance between reflection planes, θ is the reflection angle, λ is the source wavelength and *n* is an integer. A scan of multiple wavelengths or diffraction angles identifies several planes which can be used to reconstruct the crystallographic structure.[51]

$$2d \sin\theta = n\lambda \tag{2}$$

Using powder XRD in an idealized crystal would result in diffraction peaks with absolute sharpness (no width). In practice, instrumentation, source beam faults, crystal strain, temperature and crystallite size affect the breadth, shape and location of diffraction peaks.[51] Diffraction peak width is of interest in FT cobalt catalysts as the metallic cobalt is expected to be found as nanoparticles. The extent of peak broadening (β) is empirically related to the average crystallite size (τ) by the Scherrer

equation, which assumes no instrumental or strain related broadening (equation (3), where θ is the reflection angle and K is a structural factor:

$$\tau = \frac{K\lambda}{\beta \cos\theta} \tag{3}$$

A simple approach to applying the equation is to analyse a standard sample such as LaB_6 to eliminate instrumental factors. This has been used in several publications to estimate the size of nanoparticles including the pre-reduced cobalt oxide and metallic cobalt particles. The most common use for XRD in FT catalyst characterization is to determine the phase composition within a catalyst and its support.[18,25,42,53,57–59]

Adsorption - Desorption Analysis

Analysis of porous structures requires methods which can probe a significant amount of sample material without suffering from the deficiency of direct methods such as electron microscopy or local diffraction. Gas adsorption and desorption methods are used to analyse the average surface area, pore size and pore volume. Static setups based on the physisorption of N_2 close to its boiling point are widely used in conjunction with Brunauer–Emmett–Teller (BET) theory to characterize these values. A schematic drawing on the formation of adsorbed layers is shown in Figure 12. For example: catalyst supports tend to be very high surface area particles with surface areas ranging from 10–1000 m^2/g, with pore diameter ranging from 1–100 nm.

With aid of precise calibrations and measurements of pressure, temperature and volume the amount of adsorbate, the time-domain for the adsorption and desorption process can be accurately determined. Desorption being an activated process gives also an appropriate mean of studying temperature programmed desorption (TPD). Using similarly accurate setups gas phase titration of adsorbed hydrogen by oxygen pulses is used to determine the available surface sites for instance.[13,60]

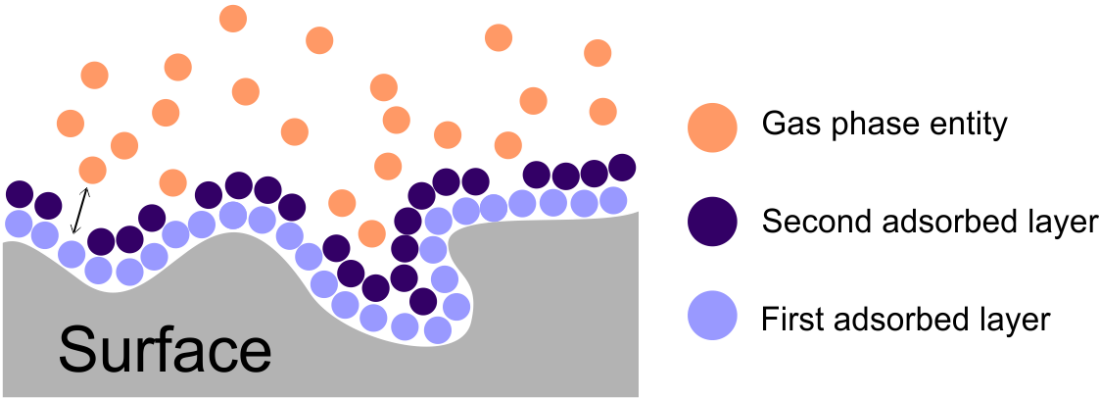

Figure 12. Schematic representation of 2 layers adsorbed on a generic surface, the gas phase entities are essentially at an equilibrium with the surface, species being constantly adsorbed and desorbed. In this case the first layer would be almost static due to presence of second layer, the adsorption energies of the layers increase with depth.

Similarly, temperature programmed reduction (TPR) can be used to determine the range of reduction and the activation energies for the reduction to take place. TPR is used to characterize the effect of promoters and support in Co-catalyst reduction and is a valuable tool to determine whether there is a strong interaction between catalyst and support, or the expected reduction ranges. In TPR a sample of analyte with precisely measured mass is loaded into a tube, the sample space if flushed with inert gas and a set flow of reductive gas is passed through the sample space. The temperature is increased slowly and the gas composition in the outlet is measured, from the decrease in the amount of reducing component, or detection of some reduction product, the reaction is characterized.[61]

Chromatography and mass spectrometry

Chromatography and mass spectrometry are advanced methods providing an indirect mean of characterizing the catalyst. This is because knowledge of the different species of product provide insight into the polymerization reaction, selectivity and reaction pathways of the catalyst and process.[62]

Perhaps the most widely used characterization techniques in FTS is chromatography. The application of a gas chromatographer (GC) can be used to qualitatively describe the product distribution obtained from FT catalysts precisely. In chromatography different compounds are separated based on their interaction with a medium,

typically in a long column, and based on the time-of-retention, duration and amounts the different fractions can be determined based on standard reference analytes. The GC information combined with overall mass balance allos the quantitative characterization of the process.[13] The products formed through FTS are a physically fractionable mixture of hydrocarbons and due to the simplicity of the method it is widely applied.[13,18,62]

The use of a mass spectrometer (MS) in conjunction with GC (GC-MS) and 2-dimensional GCxGC can be used to identify complex mixtures of each species in FT-studies. The working principle for a MS is using a high current to break, and ionize, the analysis sample (atom or molecule) into charged particles which are then quantified by their mass and charge on a variety of arrangements. These arrangements can use Time-of-Flight (ToF), a mass filter sweep or sectorized detectors to achieve the mass/charge separation. 2-dimensional GCxGC analysis allow better resolution and speciation in the analysis by separating overlapping components in using different eluents.[62]

A variation of MS is secondary ion mass spectrometry (SIMS), which provides a mean of profiling the elemental composition of a catalyst directly. Highly accelerated inert ions such as argon are used to bombard a surface which generates secondary ions based on the composition of the surface, these are then quantified by mass, charge and ToF detectors. The method provides a simple and fairly robust means of profiling elemental composition based on depth. SIMS is capable of quantifying elements in the ppb range, including the light elements.[10,13] Due also to the stochastic nature of the catalyst surface a wide area analysis by SIMS could be useful to characterize both the uniformity and profile of a much larger sample.

3. Materials and Methods

The basic cobalt catalysts LSC-59-60 and LSC-61 (Technical Research Centre of Finland VTT Ltd., 2017) used for this work are a Si-modified (1 wt%), 30 wt% Co / 0.1 wt% Pt impregnated catalyst supported on γ-Al_2O_3 Puralox® SCCa 5/150 (Sasol Germany GmbH), and the same catalyst without added Pt. Cobalt and platinum were added from their nitrate forms by incipient wetness impregnation (IWI) and mass percentages are based on the weight of the dry support and metallic forms of the additives. Both cobalt and platinum are added in two steps, each step followed by calcination at 400 °C. Addition of Si to the catalyst was made by impregnation with an ethanol solution containing 0.12 g/cm^3 tetraethyl orthosilicate and drying in air. The unmodified catalysts for this work were given as is, and the only modification realized to them was the atomic layer deposition (ALD).

The ALD of the catalysts was realized in a Picosun SUNALE™ R-200. The reactor is equipped with 4 input sources, 2 of which can be heated. Alumina was deposited on the catalysts using trimethylaluminum (TMA, SAFC, purity 99 %) and water (Milli-Q) as precursors. Platinum was deposited using trimethyl(methylcyclopenta-dienyl)platinum (MeCpPtMe3, Sigma-Aldrich, purity 99 %) and oxygen (99.9999 %) as precursors, nitrogen (99.9999 %) was used as inert purge gas. TMA and Pt precursor were handled in inert argon atmosphere glove-box to avoid spoiling the precursors when loading the source containers. The deposition cycles consisted of several short pulses of each precursor to guarantee a good surface coverage. Each deposition cycle for alumina consisted of 50 times, 0.1 sec, pulses of TMA followed by a 720 sec nitrogen purge, and 50 times, 0.1 sec, pulses of H_2O followed by a 650 sec nitrogen purge. Reaction temperature was 150 °C for alumina deposition. Each deposition cycle for platinum were 50 times, 2 sec (+5 sec stop-flow), micropulses of MeCpPtMe3 followed by a 720 sec nitrogen purge, and 50 times, 0.1 sec, micropulses of O_2 followed by an 800 sec nitrogen purge. Reaction temperature was 300 °C, system pressure was fluctuated between 8-12 hPa and carrier N_2 flow was kept at 50 sccm for all precursors. Different thicknesses were achieved by increasing number of cycles. Test pieces cut from a clean silicon wafer were put in opposite ends of the

reactor to measure film thickness achieved in each deposition process. Ellipsometry measurements of the ALD alumina test pieces had a variance of up to 20 % which is acceptable at low deposition cycles. Wafer variance, macroscopic defects and warping can lead to changes in the order of a few nanometres, which is significant when the targeted deposition is roughly 0.5, 2 and 4 nm thick, a refractive index model is not attempted for Pt growth. The catalyst variations used are presented in table 2.

Table 2. Catalyst variations used or prepared for this work and their composition

Sample	Composition
LSC-59-60	30/0.1 wt% Co/Pt on γ-alumina support
LSC-61	30 wt% Co on γ-alumina support
ALD40Alu	40 cycles ALD alumina on LSC-59-60
ALD20Alu	20 cycles ALD alumina on LSC-59-60
ALD5Alu	5 cycles ALD alumina on LSC-59-60
ALD5Pt	5 cycles ALD platinum on LSC-61

Fixed-bed Catalyst Reactor

For testing the actual running characteristics of each catalyst, a new Microactivity-Effi (PID Engineering, 2018) assembly from PID Engineering was used. The assembly consists of a reaction, feed and sampling unit. The reaction unit is composed of a hot-box fitted with twin microreactors tubes capable of being heated and cooled. The feed unit contains individual mass controllers for flow control of input gases (H_2, CO, CO_2 and N_2). Purity of H_2, CO and N_2 is 99.999 %, 99.99 % and 99.999 % respectively. The sampling unit consists of low dead-volume liquid liquid gas separators for sampling of reaction products water and liquid hydrocarbons in separate outlets while gas is allowed to flow to the assembly outlet. Wax samples are collected for the whole run to a wax trap located immediately below the reactor tubes. After each run the wax fraction collected from the wax trap are weighted to estimate the wax production of each catalysts. Outlet gases are analysed by an online GC. A picture of the Microactivity-Effi assembly is shown in figure 13 below.

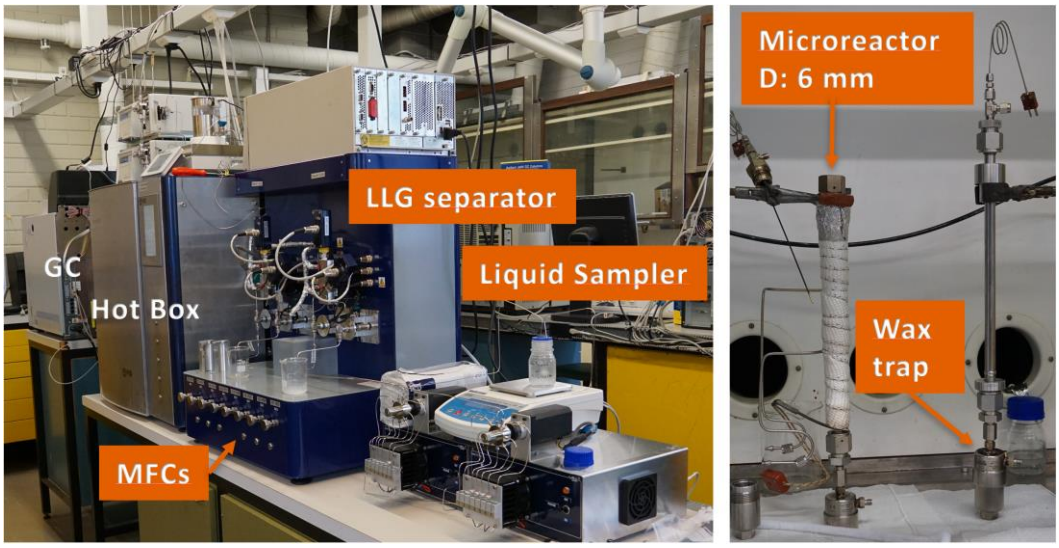

Figure 13. A picture of the Microactivity-Effi assembly as used in this work. Several features are highlighted. Reactors are housed in the hotbox during runs and online-GC is placed on the outlet of the assembly.

Approximately 1 gram of catalyst was poured to the reaction tubes (internal diameter 6 mm) giving a bed height of approximately 8 mm. The reactors are packed with quartz wool on top and below the catalyst to avoid the bed from moving in pressure discharges. The catalyst packing is illustrated in figure 14 below.

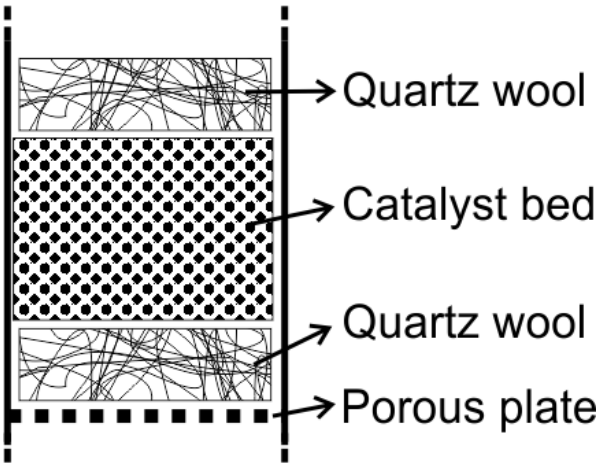

Figure 14. Catalyst packing in the reactor tube; catalyst is surrounded by quartz wool and sits atop a porous plate pressed into the reactor tube.

The bulk of the main experiments realized in the Microactivity-Effi were done at 19 barg, 200 °C and 220 °C with 90 sccm H_2, 45 sccm CO and 15 sccm N_2 gas flows. Before flowing the reaction gases into the reactors each catalyst was reduced in H_2 flow. The reduction was performed in-situ by flowing 100 ml/min of pure H_2 through the reactor for 8 hours at the specified temperature.

Characterization

Analysis of the morphology and elemental distribution of the catalysts was realized by a Merlin scanning electron microscope (Carl Zeiss, Gemini I column, 2008) equipped with a Thermo Fisher UltraDry energy dispersive X-ray spectrometer (Silicon drift detector). In-lens detector images were taken with low acceleration voltage (0.6-2 kV) to reduce charging effects, while EDS analysis was performed with a 10 kV acceleration voltage, enough for exciting relevant photons from the samples while maintaining stability. Samples were prepared for the microscopy by running a spatula over the catalyst powder in a petri dish, causing some of the particles to split revealing the interior of the catalyst. The sample was then glued to carbon tape. There are several sources of error which are difficult to quantify. Straightforward assumptions are done for EDS were a conservative 1-sigma error is assumed. This is a high error margin, but conservative, as no internal standards were used to quantify the margins.

XRD analysis was performed by a PANalytical X'Pert PRO MPD Alfa-1 instrument using a Cu Kα1 radiation source (lambda = 1.54056 Å). Sample holder diameter was 16 mm, incoming beam mask 10 mm, and a PIXcel detector was used in all measurements. For samples available in low amount an amorphous glass was used to reduce the volume of material in the holder. Step size of 0.026 ° and collection time of 1.25 sec is used for the data collection.

Software Match! (V3.6.2.121, Crystal Impact, 2018) is used to calculate average crystallite size and compare diffractograms to structures catalogued in Crystallographic Open Database (COD)[63–66]. Scherrer equation is used within Match! to calculate crystallite size from most significant peak. Instrument factor (β) is extracted from a LaB_6 standard measured with the instrument over 24 hours and fed as standard sample in software. XRD analysis are not corrected for zero-peak position, nor have the PHD values of the measurements been optimised. This lack of optimization may lead to distortions in the diffractograms at lower angles, this factor is not critical as the Scherrer-equation is applied to peaks between 40-80 degree. Yet

small variances in the peak profile and fit can have a significant effect on average crystallite size, at most 15 %, an estimation based on the XRD profile containing 5 significant peaks at distinct locations.

XRF analysis was performed in a PANalytical Axios mAX XR with a WDXRF spectrometer. The analysis was performed using a standardless method in the 15-90 kV energy range. Samples for XRF were prepared by adding around a gram of catalyst to a sample cup with a mylar film as the window.

Product analysis of the separated fractions was realized by different gas chromatographers. Wax fraction was qualitatively analysed by a HP2020 GC with in-column injection. Only paraffins are identified in this method, carbon number elution times are calibrated from known wax samples. Gas fractions were analysed from the outlet of the Microactivity-Effi assembly by a Shimadzu GC2010 with both a Flame Ionization Detector (FID) and a Thermal Calorimetric Detector (TCD). Nitrogen is used as internal standard for TCD. Inlet gas is analysed from reactor bypass prior to the run series allowing conversion calculations from TCD peak integrals and product fractions from FID peaks with known elution times. GC-data uses inert nitrogen as internal standard, thus small various in flow-rates due to pressure fluctuations can be accounted for by scaling the values according to nitrogen. Larger variance for individual GC samples is caused by fluctuations in pressure causing temperature to drop and rise momentarily affecting the output composition unpredictably. The conversion results are thus more reliable than alpha values and speciation from the online GC.

BET adsorption tests were performed in a 3Flex (Micromeritics, 2018) system using N_2 at a bath temperature of 77.3 K and 5 sec equilibration intervals.

All the quantitative results obtained as part of this work are presented in Appendix 1 & 2 for further reference. Results for the XRF measurements are given for comparison with EDS quantitative data but are otherwise left unused in this work.

4. Results

The following summarizes all experimental conditions used in the fixed-bed reactor. At least productivity and selectivity were characterized for all runs, while the catalyst from more significant runs was characterized further. The results of these characterization methods are presented in parts.

Table 3. Set of experiments run through the Microactivity-Effi and the specific parameters for each run

Run	Sample	Reduction T (°C)	P (barg)	Temperatures (°C)	Flows (sccm)
003	LSC-59-60	300	19	200, 210, 220	60:30:10 H_2:CO:N_2
004	LSC-59-60	400	19	200	90:45:15 H_2:CO:N_2
005	LSC-59-60	300	19	200	90:45:15 H_2:CO:N_2
006	LSC-59-60	300	19	200, 220	90:45:15 H_2:CO:N_2
007	LSC-59-60	400	19	200, 220	90:45:15 H_2:CO:N_2
008	ALD5Alu	400	19	200, 220	90:45:15 H_2:CO:N_2
009	ALD5Alu	400	19	200, 220	90:45:15 H_2:CO:N_2
010	ALD20Alu	400	19	200, 220, 230	90:45:15 H_2:CO:N_2
011	ALD20Alu	400	19	200, 220, 230	90:45:15 H_2:CO:N_2
012	ALD40Alu	400	19	200, 220	90:45:15 H_2:CO:N_2
013	ALD5Pt	400	19	200, 220	90:45:15 H_2:CO:N_2

Gas Chromatography

Conversion is given as percentages of either CO or H_2 converted from inlet gas mass. The graphs in Figure 15 show conversion for runs (007-013) at the main temperature set-points 200 °C and 220 °C. Variance among tested catalysts is of < 5 %-points and the values are consistent comparing CO and H_2 conversions. ALD5Alu runs showed very high conversions at given temperatures, with exception of Run009 at 220 °C. Negative values indicate a poor calibration.

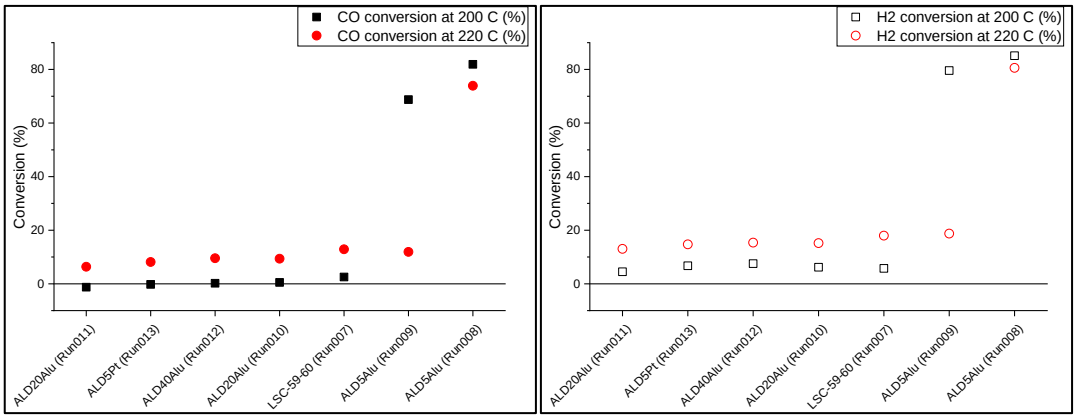

Figure 15. Conversions of hydrogen and carbon monoxide in the temperature setpoint conditions of 200 and 220 C, the conversion ranges are roughly similar, except ALD5Alu which has a very high conversion at the setpoint temperatures. Left: CO conversion; Right: H_2 conversion. High conversion combined with a high alpha value would be an indication of a good catalyst, which is not the case for ALD5Alu catalysts.

Production of wax for each catalyst for which wax could be quantified is shown in Figure 16. The productivity is normalized for amount of catalyst used in the run and rationed against time-on-service (ToS, hours). The productivity is also plotted with the alpha value calculated from GC analysis of each wax sample. Higher wax productivity is obtained from LSC-59-60 with exception of ALD20Alu. Highest alpha value estimated from the wax product is found for ALD40Alu catalyst, which had low conversion based on online-GC data. The wax productivity calculated could vary significantly between the parallel reactors due to the temperature in the wax traps affecting whether the wax condensates in the trap or if part of it moves to the piping.

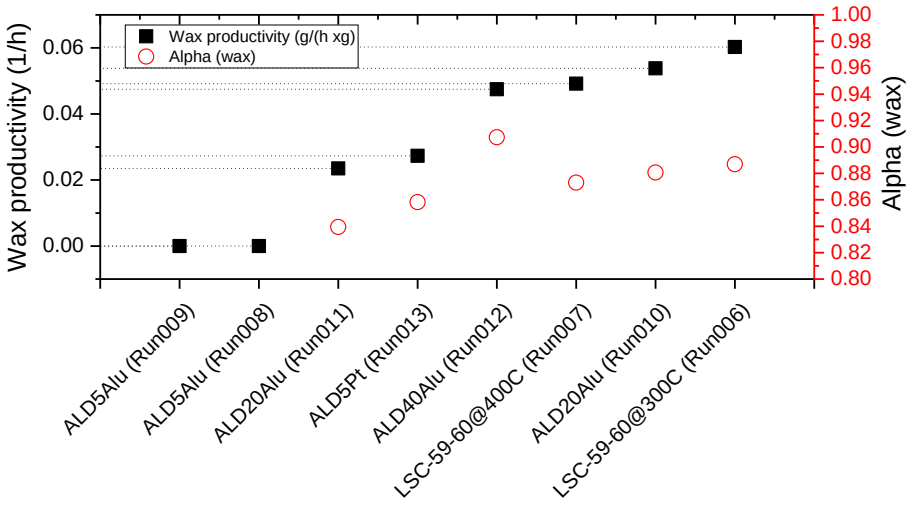

Figure 16. Wax productivity normalized to mass of catalyst & time-on-service and alpha values as calculated from wax fractions; ALD5Alu samples did not produce any waxes, while highest productivity is obtained from LSC-59-60 reduced at 300 C, highest alpha is found from wax produced with ALD40Alu sample.

X-ray Diffraction

XRD diffractograms of samples as prepared is shown in Figure 17. Expected phases are found in the diffractograms and ALD deposition does not affect the results from XRD. Peaks are marked for γ-Al_2O_3 and Co_3O_4 which are the support material and expected cobalt oxide phase from nitrate impregnation.

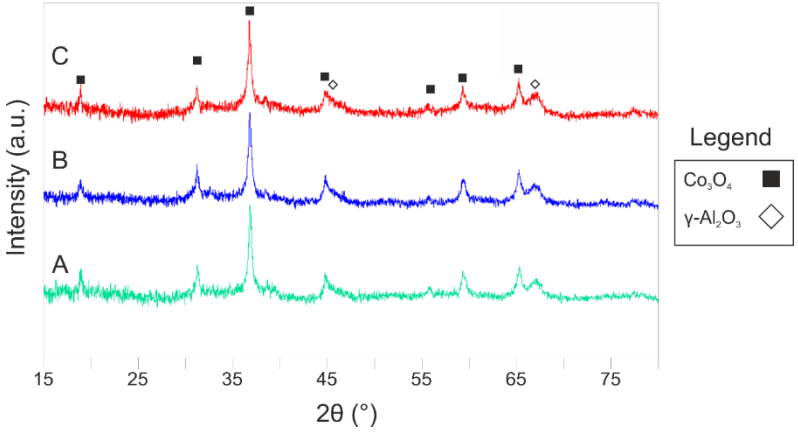

Figure 17. XRD diffractograms of A: LSC-59-60 as prepared; B: ALD40Alu as prepared and C: ALD5Pt as prepared. Found phases are cobalt oxide and γ-Al_2O_3, ALD deposition does not affect the diffractogram at these amounts. The γ-Al_2O_3 are wide and merged due to small crystallite size and the cobalt layer coverage.

XRD diffractograms are also shown for a series of samples after their respective runs in Figure 18. Notably the cobalt oxide phases cannot be identified after runs indicating a very high degree of reduction. In addition, the unmodified catalyst LSC-61 (no impregnated Pt) which was reduced at 260 °C clearly is not reduced to metallic cobalt, but to CoO with likely some Co_3O_4 remaining.

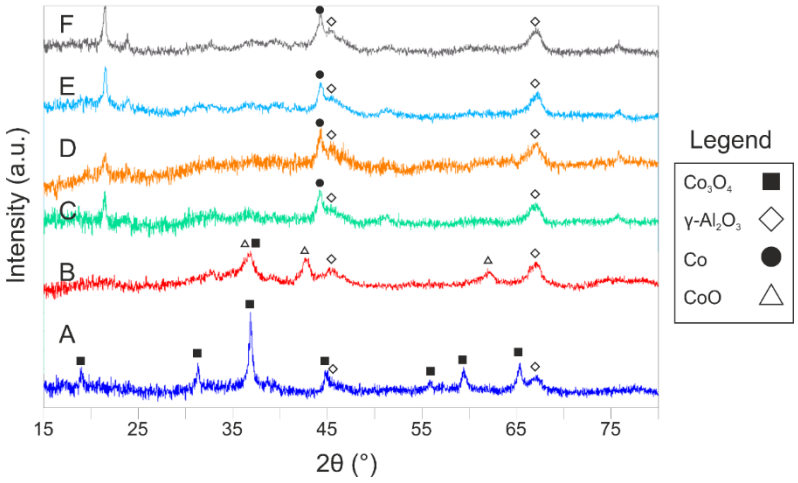

Figure 18. XRD diffractograms of A: LSC-59-60 as prepared; B: LSC-61 reduced at 260 °C; C: LSC-59-60 (Run007); D: ALD5Alu (Run009); E: ALD40Alu (Run012); F: ALD5Pt (Run013); found phases are marked on the diffractograms.

Post run diffraction shows metallic cobalt peaks at the expected locations, indicating high degree of reduction. Peaks for LSC-61 show CoO indicating poor reduction at 260 °C.

From the XRD data the average crystallite size is calculated for each of the analysed samples. The values are grouped on whether it has been in a run, or is as prepared or if the sample has been only reduced in H_2. Figure 19 shows that after reduction (even if partial) the crystallite size reduced significantly. Sample as prepared shows a large crystallite size, while samples post-run have a lower crystallite size with exception of LSC-59-60 which has larger crystallites.

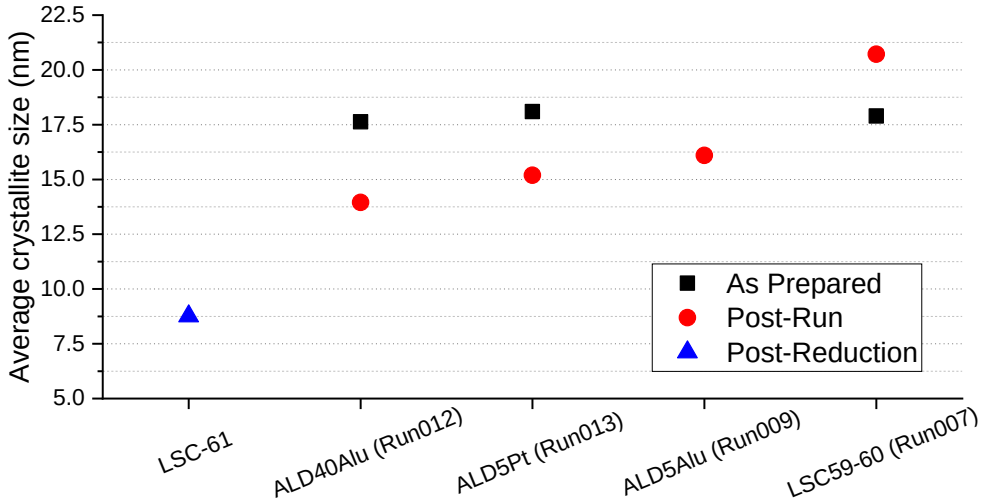

Figure 19. Average crystallite size obtained from the Scherrer equation using the XRD analysis data. Reduction leads to significantly smaller crystallite size. As prepared samples have larger crystallites in average; LSC-59-60 shows a reverse trend with larger crystallite size after the run.

Microscopy

The performed microscopy analysis shows several of the features on the surface of catalyst in the case of pre-run, post-run and post-reduction. Figure 20 shows a collage of the unmodified catalyst LSC-59-60 prior to run and its surface morphology. Pyramidal shapes and layered growth can be observed.

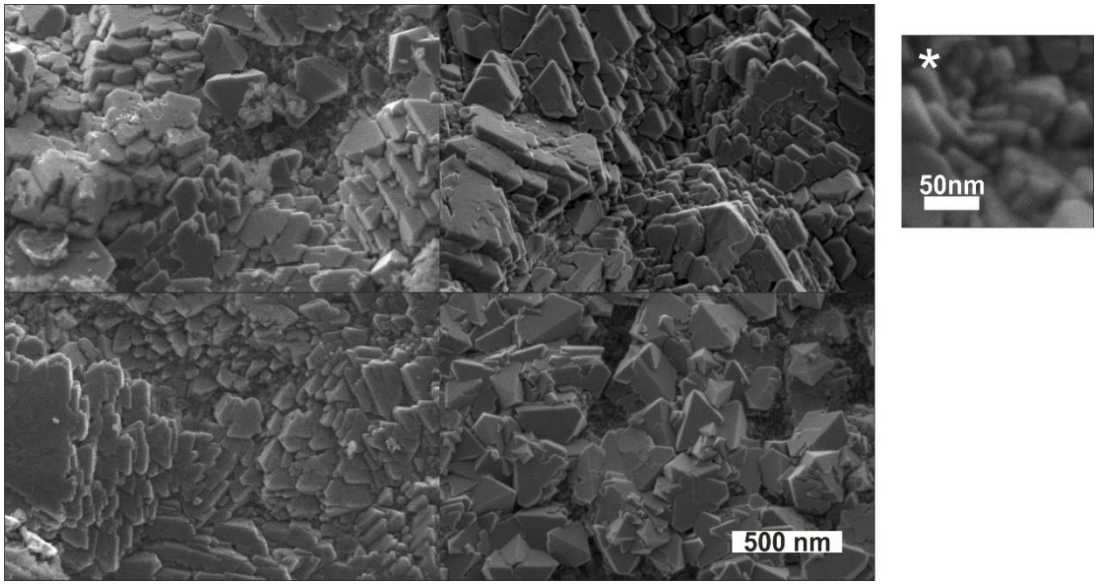

*Figure 20. SEM micrographs taken from the surface of sample LSC-59-60 as prepared. Pyramidal shapes and layered growth of cobalt oxide can be observed at the surface of catalyst particles. * Shows a higher magnification of the surface containing small protrusions.*

The cobalt distribution on the catalyst is evidenced by SEM imaging of the interface between the surface cobalt and the support. In Figure 21, below the high concentration of cobalt on the surface of the particle is contrasted to the porous support on the unmodified catalyst as prepared.

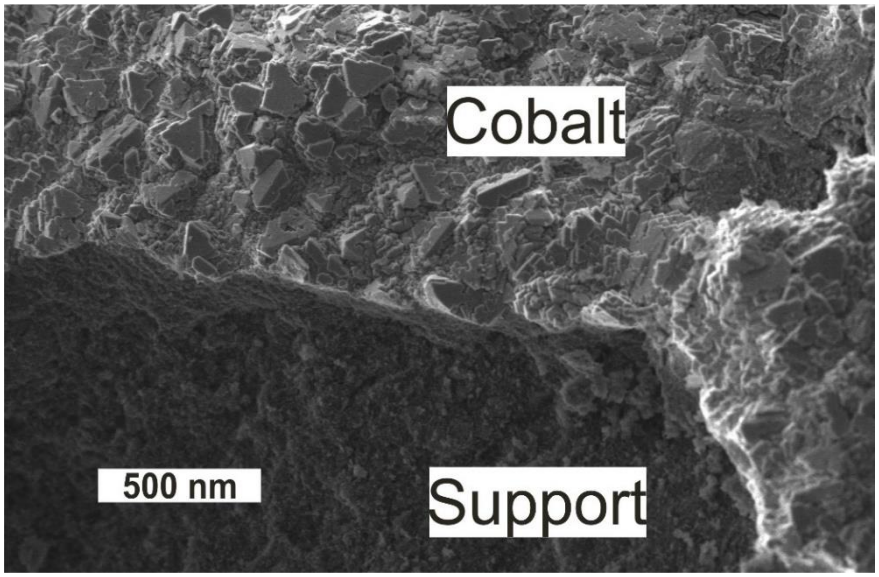

Figure 21. SEM micrograph taken from surface of LSC-59-60 sample as prepared. A piece of the surface cobalt shell has been removed by attrition exposing underlying support.

Post-run and post-reduction images clearly show changes in the catalyst surface and morphology as shown in Figure 22. The pyramidal structures found in as prepared

catalyst becomes mostly corrugated. After catalyst runs carbon deposits can be seen which cover most surface corrugations. Corrugations in post-run LSC-59-60 (reduced at 400 °C) are significantly larger than corrugations in post reduced LSC-61 and post-run LSC-59-60 reduced at 300 °C.

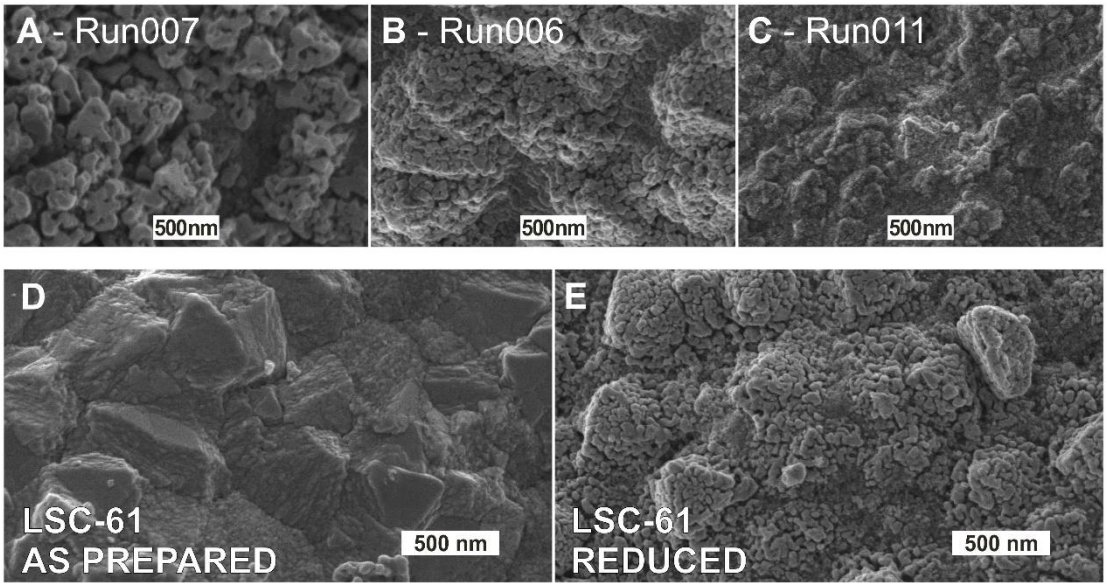

*Figure 22. SEM micrographs showing morphologies of catalysts in different states. Top-row compares catalysts post-run. Notice the size of the corrugations becomes smaller from left-to-right. On **C** the surface is covered by carbon residue, still. Bottom-row compares catalyst as prepared (**D**) to the same catalyst after being reduced (**E**).*

BET surface area

Performed N_2 BET adsorption analysis results are shown in Figure 23. As prepared catalysts have reduced surface area, both modifications with 5 and 20 cy ALD alumina increase surface area and modification by ALD Pt reduces surface area slightly. Modification with 40 cy ALD alumina simply crashes particle surface area to only 1.1 m^2/g.

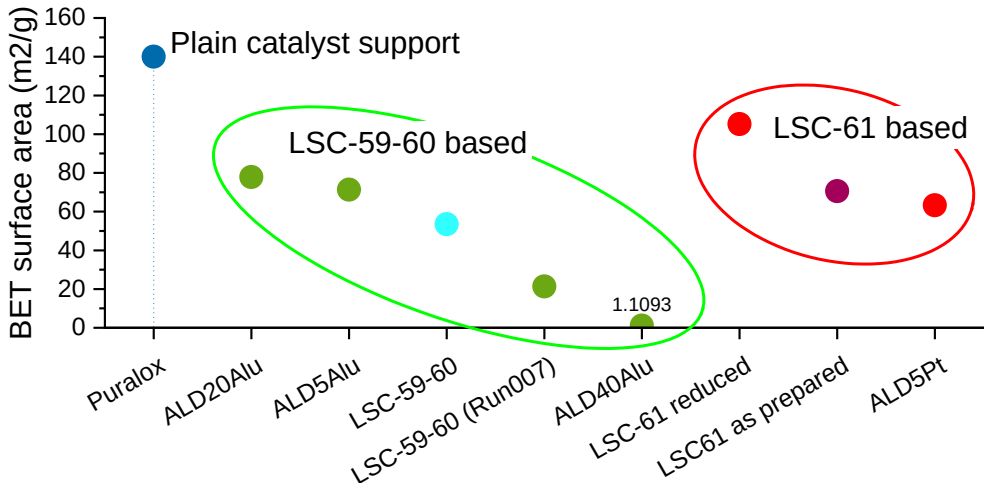

Figure 23. BET surface area of analysed samples. Results are divided in clusters based on the unmodified catalysts. ALD alumina increases surface area at least up to 20 cy, at 40 cy surface area crashes. Surface area after catalyst runs is more than halved compared to as prepared catalyst, while reduction (partial) increases surface area in LSC-61.

EDS-analysis

The interior of the catalyst particles is exposed by simply breaking the particles with a metal spatula, allowing some depth information to be analysed with SEM-EDS. The cores will tend to have a clearly higher concentration of Al and O from the support, while the outer surface will concentrate Co from the impregnation process. Local spectra collection points are shown in Figure 24 as an example. The EDS semi-quantitative analysis is tabulated in Appendix 2 for different catalysts and categorized based on interior or exterior. The semi-quantitative data is omitted from the results section because its relevance is nil compared to the elemental mappings.

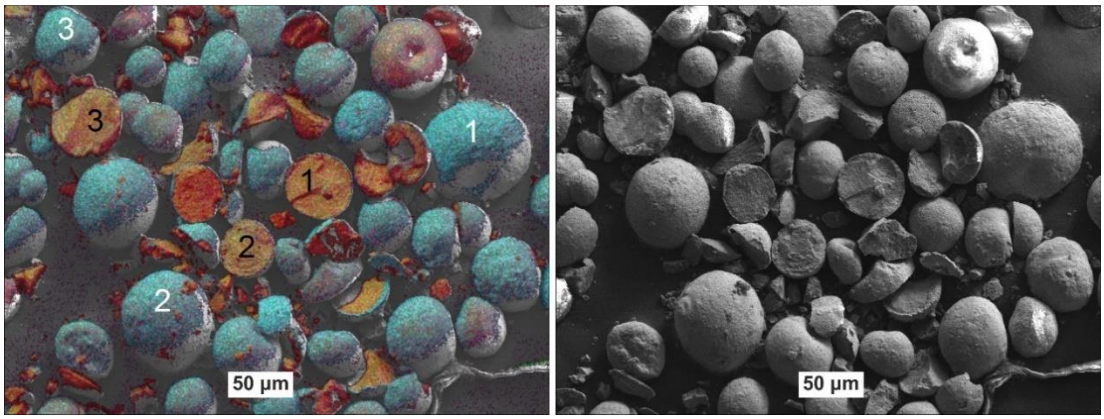

Figure 24. EDS spectral image (left) and original micrograph (right) of unmodified catalyst giving an overview of the catalyst composition and locations from which quantitative data is extracted. Black numbers are for regions in the center of the particles, while white numbers are from the surface of particles. Quantitative data is an average of these spectrums. Colours in spectral image: Co – cyan, O – red, Al – green and Pt – magenta.

The exposed central area of a catalyst particle and the mapping of different elements can be seen in Figure 25. From the elemental mapping a clear egg-shell type cobalt distribution can be discerned. The Co is strongly mapped to the outer surface of each particle while the center has a much higher abundance of Al and O (alumina).

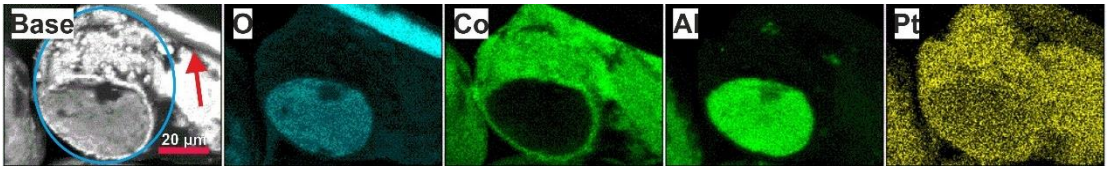

Figure 25. Base SEM image and elemental maps of a single halved cobalt particle (LSC-59-60 post-run) showing the egg-shell structure and distribution of elements as labelled. The colour intensity in each map is arbitrary, Pt map highlights the almost homogeneous origin of EDS counts. The red arrow points to a stray quartz strand.

The SEM image and elemental mapping for the unmodified catalysts and the ALD Pt modified catalyst is shown in Figure 26. The elemental maps showed: a uniform distribution of cobalt on the interior of the particles and the egg-shell distribution for all catalysts (Figure 26, arrows); that the amount of cobalt in the surface of each particle varied, differences which are visually discernible from the maps (Figure 26, hexagons); and that the ALD5Pt catalyst showed a positive correlation between Pt amount and lower amount of cobalt on surface (Figure 26, circles).

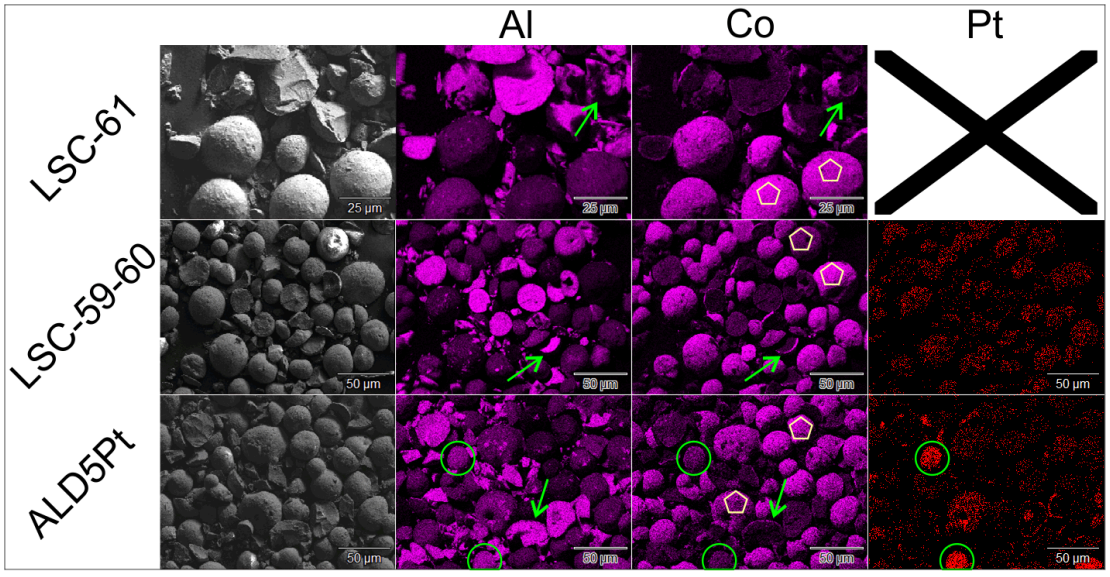

Figure 26. SEM image and the respective EDS elemental mapping for samples LSC-61, LSC-59-60 and ALD5Pt. Highlighted features are egg-shell Co distribution (arrows), visible variance in surface Co concentration (hexagons) and higher Pt concentration in areas of lower Co concentration (circles).

5. Discussion

Reactor Performance

During the experimental part of this work shortcoming were identified mainly in the lack of reproducibility between the parallel reactors. The results obtained in parallel runs with respect to productivity, selectivity and activity varied so significantly that uncertainty with respect to several parameters cannot be ignored. Thus, some simplifications and assumptions were made for this discussion. Regarding characterization the SEM, EDS and XRD analysis gives a framework to compare the catalysts before and after each run, while reactor data and online-GC were the only means of engaging with the catalyst during the run. The analysis before, during and after each run can be cross-linked, but it is important to notice the data is taken at face-value. One example of the issues is found in the conversion and productivity values for runs 003 to 007 (see Appendix 1), which should be roughly the same for tests which have been repeated, since reaction conditions and the catalyst used are identical. This gives an indication of process related issues in the extraction of wax from the systems and in the parallel reactor operation. Also the catalysts ALD5Alu and ALD20Alu were run in parallel presumably with the same parameters, but the results showed significant disparity. The difference is likely due to the actual operating conditions of the reactor tubes as opposed to differences in the catalyst properties. The discrepancy is large enough that from the comparable runs in the reactor the catalytic activity should not be correlated with production of wax, nor with the alpha values obtained from the extracted waxes. Each value should be treated separately.

ALD Alumina

Deposition of ALD alumina on the samples was expected to reduce sintering. The results obtained through XRD analysis (Figure 19) and microscopy (Figure 22) show that there is a negative trend in average crystallite size and the scale of the corrugations in the catalysts surfaces as the ALD alumina load increases. With higher alumina loadings the average crystallite size and corrugations are smaller. The results

are interesting considering the ToS of the catalysts, which was higher for ALD40Alu catalyst (>70 h) as compared to unmodified catalyst (60 h). Appropriate to mention the XRD diffractograms obtained in this work match remarkably well with the diffractograms presented in Garces, L. et al[42]. This is expected as cobalt over alumina support is used in both works. Although there is no in-situ XRD during the reduction and during the initial activity stages, it is very likely the ALD coating is stabilizing cobalt particles during initial activity. As an undocumented parameter the ALD5Alu catalyst overshot in temperature to 270 °C for a period of 10 hours, nevertheless the average crystallite size is smaller than in the case of the unmodified catalyst.

Instead of simply having a passive role during the tests, the 5-cycle load of alumina increased methanation and activity for an extended period, as shown by the high conversion (see Figure 15 & Appendix 1). This activity was equivalent to the initial activity encountered on any of the catalysts, but seemingly had no fall-off for as long as 40 h. A hint to a possible activity fall-off can be seen in the conversions at 220 °C for one of the ALD5Alu runs (Figure 15), which are an average of the conversions during the last 4 hours of the run. This does give an indication of a more intimate interaction between alumina and cobalt surface. The work on alumina supported cobalt catalysts for aqueous phase reactions by Lee, J. et al tried using ALD alumina as a top-coating, but found formation of non-catalytic cobalt aluminates during calcination; claiming calcination as a necessary step to open accesses to reaction sites.[23] However, in our work none of the catalysts where calcinated following ALD deposition. Even at 40 cycles of ALD alumina diffractograms (Figure 18) showed very consistent phase composition after each run for cobalt (metallic cobalt). No issues could be identified during the deposition of ALD alumina and included silicon test pieces had a uniform coating distribution while microscopy did not reveal any disparities. In case of severe CVD like growth a thick overcoat would be expected throughout the catalyst following the direction of the catalyst bed, which should be identifiable during microscopy. Also, the simple observation that there is no remnant cobalt oxide peaks in XRD (Figure 18) indicates most of the cobalt is still accessible to hydrogen during reduction. It is possible, however, that the coatings are non-uniform

towards the centre of the catalyst particles as this cannot be confirmed without further investigation by more advanced methods such as TEM or XPS.

BET analysis clearly shows a dramatic fall-off in surface area at the 40-cy alumina loading, while 5 and 20 cy alumina loadings show a reversed trend of increased surface area (Figure 23). The deposited alumina is seemingly porous, allowing hydrogen diffusion during reduction. For the ALD40Alu catalyst it is possible the outer pores are simply covered and the BET analysis is not reliable due to the interior of the particle not being accessible with the measurement conditions. The previous raises an interesting question on whether the majority of the activity, which is comparatively low, in the ALD40Alu catalyst originates from the outer surface, the porous interior, or both the interior and exterior of the catalyst particle. Despite the lower activity, a significant fraction of waxes was produced, and these waxes had a higher alpha value compared to the other catalyst variations (Figure 16). At face-value this indicates that at the higher loads the ALD alumina could be binding to sites which are not contributing to chain growth.

ALD Platinum

Platinum assists in the reduction and hydrogenating properties of cobalt catalysts. This is a well-supported observation and is also corroborated in this work. The slightly lower alpha value and lower wax-productivity value (Figure 16), and higher paraffin fraction compared to unmodified catalyst (see Appendix 2) indicate a higher hydrogenation rate while having a similar conversion. Based on the XRD data the reduction of the ALD5Pt catalyst is on par with the reduction of the Pt impregnated catalysts as no cobalt oxide peaks are identified and intensities are similar. The results are interesting since the ALD deposition is limited to only 5 cycles. Assuming the deposition process proceeded as designed an even smaller amount of ALD platinum would serve to achieve the reduction target and increase alpha values. The EDS results hint to a possible excess of platinum on the surface of the catalyst (0.3–2.6 wt%), but otherwise an essentially nil amount of platinum in the porous core. EDS analysis of the unmodified catalyst showed a smaller Pt concentration on the surface

of the catalysts (0.1–0.2 wt%) and similarly a nil amount of Pt in the core (see Appendix 2). Furthermore, the BET surface area showed a slight decline which would indicate either a lower pore effect or a high overall coverage, but the low core Pt concentration according to EDS indicates otherwise.

Catalyst Structure

The SEM-EDS analysis shows that the impregnation step of the unmodified catalysts results in an egg-shell type of structure, where most of the impregnate is in the very surface of the support particle (). This is typical for a single step impregnation where the impregnate is loaded from a super-saturated solution. Regardless of the shell having most of the cobalt, the interior of the support particles contains a uniform amount of cobalt throughout according to EDS analysis of particle cross-sections. The as prepared cobalt average crystallite size is taken to represent a rough estimation of average cobalt particle size. The values are likely over estimations as the pore size of the support (measured from desorption for the batch used in this work) is around 12 nm. This would set a relaxed upper boundary to the crystallite size. The values are realistic enough and the amount on the surface of the catalyst is such that this average crystallite size can be taken as a realistic representation of the whole catalyst body. The assumption is very similar to the conclusion reached by Chu, W. et al[15] which found that XRD data overestimates the particle size as compared to other methods such as microscopy.

Activation and Deactivation

The data collected in this work is from such a short time span it is essentially impossible to observe long-term deactivation in the catalysts. Run times were limited to no more than 70 h due to the wax trap becoming overfilled, causing wax to clog the system. Even though most catalysts suffered from rather high temperature spikes (> 250 °C) these did not seem to be enough to deactivate any of the catalysts. All of runs with the unmodified catalysts were productive and temperature spikes could not be correlated with conversion. In some catalysts it seemed large sudden changes

in pressure were responsible for their deactivation, but this assertion is rather speculative. The only exception to high initial activity, typically lasting < 10 h was the ALD40Alu catalyst, which showed no temperature spike. By themselves the catalysts used would not reach equilibrium, active cooling was necessary for the catalysts to find a new thermodynamic equilibrium. This indicates the chemistry of the surface sites might evolve such that quickly hydrogenating defect free planes become more inactive, while chain growing defects are not significantly affected.

6. Conclusions and Future Work

6.1. Conclusions

We investigated the modification of an impregnated cobalt catalyst by ALD deposited alumina and platinum for Fischer-Tropsch synthesis. The effects of both types of coatings was observable.

The alumina depositions are found to reduce the average crystallite size, which is possibly due to reduced sintering and stabilization of smaller particles. Alumina was also found to affect the wax productivity negatively at the lowest load, while having the opposite effect at the highest load used. No literature investigation in this author's knowledge makes such a claim in the topic of FTS catalysts, thus caution is advised, and slight optimism practiced.

The ALD platinum load used affected alpha values and wax productivity negatively, this is attributed to the high effective load of platinum introduced due to the nature of ALD depositions compared to impregnation. The effects of platinum are in sound agreement with findings from literature[8,15], and the potential of Pt ALD with single digit cycles is shown.

Our experiments were not enough to give any indication on long-term deactivation in terms of conversion. The effects of either deposition on deactivation was thus not determined in any practical capacity. Although several characterization methods were employed, to observe long-term deactivation with the used experimental conditions the run time of each catalyst would have to double. On a focus experiment the long-term deactivation could be accelerated significantly by using i.e.: higher reaction temperatures.

High initial activity, observed as a strong exothermic period lasting up to 10 hours, was found for all catalyst experiments except ALD40Alu catalyst. During this stage temperatures reaching above 250 °C with differences on duration were observed, but no conclusions are made concerning this stage due to lack of systemic methods to analyse this phase in the catalyst lifetime. To quantify the activation phase of the

catalyst in-situ XRD combined with precise dosage of precursors would be a potential option, this could relate the reaction rate with the crystalline structure, which is assumed to change dramatically within the activation period. It would also be important for the temperature control to be very consistent throughout the different experiments, which was not the target in our experiments were keeping the catalyst from overheating was the priority.

Most analytical methods used proved useful for this work. An exception to this was the XRF, in which the procedure was realized without any standards and thus the results were left mostly unused. Electron microscopy, EDS, BET surface area and XRD supported each other's results synergistically forming a cohesive suit of analytical methods for catalyst characterization before and after each run. This work hopefully has reinforced the need and possibilities of such characterizations.

The goals of this work have been fulfilled regarding development of catalyst characterization frameworks, and the results can be used to steer further catalyst development with the intent of producing heavier wax products. Optimistic conclusions for the use of both ALD alumina and ALD platinum in further catalyst development was found even though faults involved in the preparation and experimental runs diminished the overall value of work.

6.2. Future work

First and foremost, the reproducibility of the results needs to be assured with at least one experimental run. This would validate the results obtained in the Microeffi experiments. Concerning catalyst variations lower loads of ALD platinum are needed, and validation of the ALD deposition would be of advantage to the credibility of the process. The latter can be achieved by TEM and XPS analysis verifying whether deposition rates are in acceptable ranges.

Catalyst characterization needs to include chemisorption to analyse the interaction between ALD alumina and the catalyst at different loads, leading to an understanding of why top-coatings do not necessarily diminish activity. Reduction followed by in-

situ chemisorption would be particularly interesting in determining the active surface sites of the different catalysts used. XRD analysis on unmodified catalyst post-reduction and analysis of non-promoted LSC-61 would serve to complement the data on average crystallite size. Further XRD of ALD20Alu post run would allow even a crude linear model to be developed for the effect of ALD alumina on crystallite size.

From a broader point-of-view the work with ALD aluminium and/or other top-coatings is presently the more novel path to investigate compared to low-loadings of promoters through ALD. The inherent advantages of ALD for digitally controlled films is well established, but the modification of active thin films grown on random microporous substrates has not been widely studied yet. If the effects of the top-coatings improve other aspects in the catalyst such as alpha values and wax productivity these catalyst modifications would prove very effective for FTS of high value products.

7. REFERENCES

1. De Klerk, A., Li, Y. W. & Zennaro, R. *Greener Fischer– Tropsch Processes for Fuels and Feedstocks*. (Wiley-VCH, 2013).

2. Speight, J. G. *Hydrocarbons from Synthesis Gas*. *Handbook of Industrial Hydrocarbon Processes* (Elsevier Inc., 2011). doi:10.1016/B978-0-7506-8632-7.10008-8

3. Schulz, H. Short history and present trends of Fischer–Tropsch synthesis. *Appl. Catal. A Gen.* **186,** 3–12 (1999).

4. Mahmoudi, H. *et al.* A review of Fischer Tropsch synthesis process, mechanism, surface chemistry and catalyst formulation. *Biofuels Eng.* **2,** 11–31 (2017).

5. van Steen, E., Claeys, M., Möller, K. P. & Nabaho, D. Comparing a cobalt-based catalyst with iron-based catalysts for the Fischer-Tropsch XTL-process operating at high conversion. *Appl. Catal. A Gen.* **549,** 51–59 (2018).

6. Speight, J. G. Fischer-Tropsch Chemistry. in *Rules of Thumb for Petroleum Engineers* 268 (John Wiley & Sons, 2017). doi:10.1016/B978-0-7506-8632-7.10008-8

7. Rytter, E. & Holmen, A. Perspectives on the Effect of Water in Cobalt Fischer-Tropsch Synthesis. *ACS Catal.* **7,** 5321–5328 (2017).

8. Rytter, E., Tsakoumis, N. E. & Holmen, A. On the selectivity to higher hydrocarbons in Co-based Fischer-Tropsch synthesis. *Catal. Today* **261,** (2016).

9. Van Berge, P. J., Van De Loosdrecht, J., Barradas, S. & Van Der Kraan, A. M. Oxidation of cobalt based Fischer-Tropsch catalysts as a deactivation mechanism. *Catal. Today* **58,** 321–334 (2000).

10. Tsakoumis, N. E., Rønning, M., Borg, Ø., Rytter, E. & Holmen, A. Deactivation of cobalt based Fischer-Tropsch catalysts: A review. *Catal. Today* **154,** 162–182 (2010).

11. Weststrate, C. J., van de Loosdrecht, J. & Niemantsverdriet, J. W. Spectroscopic insights into cobalt-catalyzed Fischer-Tropsch synthesis: A review of the carbon monoxide interaction with single crystalline surfaces of cobalt. *J. Catal.* **342,** 1–16 (2016).

12. Girardon, J. S., Constant-Griboval, A., Gengembre, L., Chernavskii, P. A. & Khodakov, A. Y. Optimization of the pretreatment procedure in the

design of cobalt silica supported Fischer-Tropsch catalysts. *Catal. Today* **106,** 161–165 (2005).

13. Haber, J., Block, J. H. & Delmon, B. Manual of methods and procedures for catalyst characterization (Technical Report). *Pure Appl. Chem.* **67,** 1257–1306 (1995).

14. Jean-Marie, A., Griboval-Constant, A., Khodakov, A. Y. & Diehl, F. Cobalt supported on alumina and silica-doped alumina: Catalyst structure and catalytic performance in Fischer-Tropsch synthesis. *Comptes Rendus Chim.* **12,** 660–667 (2009).

15. Chu, W. *et al.* Cobalt species in promoted cobalt alumina-supported Fischer-Tropsch catalysts. *J. Catal.* **252,** 215–230 (2007).

16. Chen, W., Zijlstra, B., Filot, I. A. W., Pestman, R. & Hensen, E. J. M. Mechanism of Carbon Monoxide Dissociation on a Cobalt Fischer–Tropsch Catalyst. *ChemCatChem* **10,** 136–140 (2018).

17. Weststrate, C. J., van Helden, P. & Niemantsverdriet, J. W. Reflections on the Fischer-Tropsch synthesis: Mechanistic issues from a surface science perspective. *Catal. Today* **275,** (2016).

18. Mcnab, A. I. Quantification and qualification of species adsorbed on Fischer-Tropsch catalysts. (University of Aberdeen, 2017).

19. van de Loosdrecht, J. *et al.* Providing Fundamental and Applied Insights into Fischer–Tropsch Catalysis: Sasol–Eindhoven University of Technology Collaboration. *ACS Catal.* **6,** 3840–3855 (2016).

20. Backman, L. Supported Cobalt Catalysts – Preparation, Characterization and Reaction Studies. (Helsinki University of Technology, 2009).

21. Marceau, E., Carrier, X. & Che, M. Impregnation and drying of solid catalysts. in *Synthesis of Solid Catalysts* 59–82 (2009). doi:10.1002/9783527626854.ch4

22. Lok, M. Coprecipitation. in *Synthesis of Solid Catalysts* 135–151 (2009).

23. Lee, J. *et al.* Enhanced stability of cobalt catalysts by atomic layer deposition for aqueous-phase reactions. *Energy Environ. Sci.* **7,** 1657 (2014).

24. O'Neill, B. J. *et al.* Catalyst Design with Atomic Layer Deposition. *ACS Catal.* **5,** 1804–1825 (2015).

25. Taheri Najafabadi, A., Khodadadi, A. A., Parnian, M. J. & Mortazavi, Y. Atomic layer deposited Co/γ-Al2O3catalyst with enhanced cobalt dispersion and Fischer-Tropsch synthesis activity and selectivity. *Appl.*

Catal. A Gen. **511,** 31–46 (2016).

26. Munnik, P., Jongh, P. E. De & Jong, K. P. De. Recent Developments in the Synthesis of Supported Catalysts. (2015). doi:10.1021/cr500486u

27. Johnson, R. W., Hultqvist, A. & Bent, S. F. A brief review of atomic layer deposition : from fundamentals to applications. *Biochem. Pharmacol.* **17,** 236–246 (2014).

28. Miikkulainen, V., Leskelä, M., Ritala, M. & Puurunen, R. L. Crystallinity of inorganic films grown by atomic layer deposition: Overview and general trends. *J. Appl. Phys.* **113,** (2013).

29. Jang, Y. *et al.* Highly-conformal nanocrystalline molybdenum nitride thin films by atomic layer deposition as a diffusion barrier against Cu. *J. Alloys Compd.* **663,** 651–658 (2016).

30. Chow, L. A. Equipment and Manufacturability Issues in CVD Processes. in *Handbook of Thin Film Deposition - Techniques, Processes, and Technologies* (ed. Seshan, K.) (Elsevier, 2012).

31. Knoops, H. C. M., Potts, S. E., Bol, A. A. & Kessels, W. M. M. Atomic Layer Deposition. in *Handbook of Crystal Growth* 1101–1134 (Elsevier, 2015). doi:10.1016/B978-0-444-63304-0.00027-5

32. Dendooven, J. & Detavernier, C. Basics of Atomic Layer Deposition: Growth Characteristics and Conformality. *At. Layer Depos. Energy Convers. Appl.* 39 (2017).

33. Aaltonen, T., Ritala, M., Sajavaara, T., Keinonen, J. & Leskelä, M. Atomic Layer Deposition of Platinum Thin Films. *Chem. Mater.* **15,** 1924–1928 (2003).

34. Ritala, M. & Leskela, M. Atomic Layer Deposition of Noble Metals and Their Oxides Jani Ha m. (2013). doi:10.1021/cm402221y

35. Ylivaara, O. M. E. *et al.* Aluminum oxide from trimethylaluminum and water by atomic layer deposition: the temperature dependence of residual stress, elastic modulus, hardness and. *Thin Solid Films* **552,** 124–135 (2014).

36. Shrestha, P. *et al.* Investigation of Volmer-Weber Growth during the Nucleation Phase of ALD Platinum Thin Films and Template Based Platinum Nanotubes. in **4,** 127–134 (2010).

37. Gordon, R. G., Hausmann, D., Kim, E. & Shepard, J. A kinetic model for step coverage by atomic layer deposition in narrow holes or trenches. *Chem. Vap. Depos.* **9,** 73–78 (2003).

38. Yanguas-Gil, A. & Elam, J. W. Diffusion-Reaction Model of ALD in

Nanostructured Substrates: Analytic Approximations to Dose Times as a Function of the Surface Reaction Probability. **41,** 169–174 (2011).

39. Rytter, E. & Holmen, A. On the support in cobalt Fischer–Tropsch synthesis—Emphasis on alumina and aluminates. *Catal. Today* **275,** 11–19 (2016).

40. Schulz, H. *Comparing Fischer-Tropsch synthesis on iron- and cobalt catalysts. The dynamics of structure and function*. *Studies in Surface Science and Catalysis* **163,** (Elsevier B.V., 2007).

41. Gnanamani, M. K. *et al.* Fischer-Tropsch synthesis: Effect of pretreatment conditions of cobalt on activity and selectivity for hydrogenation of carbon dioxide. *Appl. Catal. A Gen.* **499,** 39–46 (2015).

42. Garces, L. J., Hincapie, B., Zerger, R. & Suib, S. L. The effect of temperature and support on the reduction of cobalt oxide: An in situ x-ray diffraction study. *J. Phys. Chem. C* **119,** 5484–5490 (2015).

43. Wolf, M., Mutuma, B. K., Coville, N. J., Fischer, N. & Claeys, M. Role of CO in the Water-Induced Formation of Cobalt Oxide in a High Conversion Fischer–Tropsch Environment. *ACS Catal.* 3985–3989 (2018). doi:10.1021/acscatal.7b04177

44. Tompkins, H. G. & Augis, J. A. The oxidation of cobalt in air from room temperature to 467 °C. *Oxid. Met.* **16,** 355–369 (1981).

45. Lancelot, C. *et al.* Direct evidence of surface oxidation of cobalt nanoparticles in alumina-supported catalysts for fischer-tropsch synthesis. *ACS Catal.* **4,** 4510–4515 (2014).

46. Dalai, A. K. & Davis, B. H. Fischer-Tropsch synthesis: A review of water effects on the performances of unsupported and supported Co catalysts. *Appl. Catal. A Gen.* **348,** 1–15 (2008).

47. Zhang, M., De Respinis, M. & Frei, H. Time-resolved observations of water oxidation intermediates on a cobalt oxide nanoparticle catalyst. *Nat. Chem.* **6,** 362–367 (2014).

48. van de Loosdrecht, J. *et al.* Cobalt Fischer-Tropsch synthesis: Deactivation by oxidation? *Catal. Today* **123,** 293–302 (2007).

49. Gay, A.-S. *et al.* Combined characterization of cobalt aggregates by HAADF-STEM electron tomography and Anomalous X-ray scattering. *Eur. Microsc. Congr. 2016 Proc.* **128,** 39–40 (2016).

50. Wang, Z. L. & Lee, J. L. *Electron microscopy techniques for imaging and analysis of nanoparticles*. **2,** (2009).

51. Leng, Y. *Materials Characterization Introduction to Microscopic and*

Spectroscopy Methods. (Wiley-Vch, 2008).

52. Hodkiewicz, J. & Scientific, T. F. Characterizing Carbon Materials with Raman Spectroscopy. *Prog. Mater. Sci.* **50,** 929–961 (2005).

53. Zhou, W. & Greer, H. F. What Can Electron Microscopy Tell Us beyond Crystal Structures? *Eur. J. Inorg. Chem.* **2016,** 941–950 (2016).

54. Davis, J. R. X-Ray Diffraction for Bulk Structural Analysis. in *Metals Handbook, Desk Edition* (1998).

55. Claeys, M. *et al.* In situ magnetometer study on the formation and stability of cobalt carbide in Fischer-Tropsch synthesis. *J. Catal.* **318,** 193–202 (2014).

56. Tavakoli, A. H. *et al.* Amorphous alumina nanoparticles: Structure, surface energy, and thermodynamic phase stability. *J. Phys. Chem. C* **117,** 17123–17130 (2013).

57. Zhu, Y., Ye, Y., Zhang, S., Leong, M. E. & Tao, F. Synthesis and catalysis of location-specific cobalt nanoparticles supported by multiwall carbon nanotubes for Fischer-Tropsch synthesis. *Langmuir* **28,** 8275–8280 (2012).

58. Storsæter, S., Borg, Blekkan, E. A. & Holmen, A. Study of the effect of water on Fischer-Tropsch synthesis over supported cobalt catalysts. *J. Catal.* **231,** 405–419 (2005).

59. Borg, Ø., Rønning, M., Storster, S., van Beek, W. & Holmen, A. Identification of cobalt species during temperature programmed reduction of Fischer-Tropsch catalysts. *Stud. Surf. Sci. Catal.* **163,** 255–272 (2007).

60. Brunauer, S., Emmett, P. H. & Teller, E. Adsorption of Gases in Multimolecular Layers. *J. Am. Chem. Soc.* **60,** 309–319 (1938).

61. Besselmann, S., Freitag, C., Hinrichsen, O. & Muhler, M. Temperature-programmed reduction and oxidation experiments with V2O5/TiO2 catalysts. *Phys. Chem. Chem. Phys.* **3,** 4633–4638 (2001).

62. Van Der Westhuizen, R., Crouch, A. & Sandra, P. The use of GC×GC with time-of-flight mass spectrometry to investigate dienes and Diels-Alder polymerisation products in high-temperature Fischer-Tropsch-based fuels. *J. Sep. Sci.* **31,** 3423–3428 (2008).

63. Gražulis, S. *et al.* Crystallography Open Database (COD): an open-access collection of crystal structures and platform for world-wide collaboration. *Nucleic Acids Res.* **40,** D420–D427 (2012).

64. Gražulis, S. *et al.* Crystallography Open Database - an open-access

collection of crystal structures. *J. Appl. Crystallogr.* **42,** 726–729 (2009).

65. Merkys, A. *et al.* COD::CIF::Parser: an error-correcting CIF parser for the Perl language. *J. Appl. Crystallogr.* **49,** (2016).

66. Gražulis, S., Merkys, A., Vaitkus, A. & Okulič-Kazarinas, M. Computing stoichiometric molecular composition from crystal structures. *J. Appl. Crystallogr.* **48,** 85–91 (2015).

Table 4. Compilation of data obtained for all experimental runs, post-run and pre-run characterization (part 1)

APPENDIX 1 (1/2)

				GC-online												Mass			Wax-Cromatography		
#	Run	Sample	Reaction conditions	C1+C2	LPG	p 5-14	o 5-14	C15-25	oxy	CO2	para%	X_CO	X_H2	alpha	purpose	mwax (g)	mcat (g)	tTOS (h)	wax/g*h	max-Cn	alpha-wax
1	002	ALD6 - 20 cy Al2O3	200°C, 19 barg, 6 l/h	41.5	19.9	21.0	15.8	0.0	1.8	0.0	0.57	4.6	5.6	0.74	test run	4.35	1.025	58.0	0.073	48	0.894
2	002	ALD6 - 20 cy Al2O3	210°C, 19 barg, 6 l/h	42.6	20.9	22.3	13.9	0.0	0.2	0.0	0.62	8.6	10.0	0.70	test run	4.35	1.025	58.0	0.073	48	0.894
3	002	ALD6 - 20 cy Al2O3	220°C, 19 barg, 6 l/h	44.9	22.8	19.9	12.4	0.0	0.0	0.0	0.62	15.9	13.9	0.61	test run	4.35	1.025	58.0	0.073	48	0.894
4	003	LSC-59-60	200°C, 19 barg, 6 l/h	41.5	23.8	15.9	17.9	0.0	0.7	0.0	0.47	9.3	11.6	0.66	test run	8	1.027	58.0	0.134		
5	003	LSC-59-60	210°C, 19 barg, 6 l/h	39.8	25.9	14.8	19.4	0.0	0.1	0.0	0.43	22.1	25.4	0.59	test run	8	1.027	58.0	0.134		
6	003	LSC-59-60	220°C, 19 barg, 6 l/h	40.6	27.7	14.8	16.8	0.0	0.2	0.0	0.47	31.8	33.5	0.51	test run	8	1.027	58.0	0.134		
7	004	LSC-59-60 @ 400C	200°C, 19 barg, 9 l/h	46.4	0.4	0.3	0.1	0.0	0.0	52.8	0.75	98.5	100.0	0.58	test run	0	1.108	71.5	-	46	0.865
8	005	LSC-59-60 @ 300C	200°C, 19 barg, 9 l/h	59.5	1.1	0.6	0.9	0.0	0.0	37.8	0.42	62.2	71.5	0.61	test run	0	1.134	71.5	-	49	0.862
9	006	LSC-59-60 @ 300C	200°C, 19 barg, 9 l/h	34.2	23.7	17.6	23.8	0.5	0.3	0.0	0.42	6.1	9.1	0.71	test run	3.4	0.94	60.0	0.060	55	0.887
10	006	LSC-59-60 @ 300C	220°C, 19 barg, 9 l/h	42.1	27.2	17.9	12.7	0.0	0.1	0.0	0.59	27.9	33.5	0.51	test run	3.4	0.94	60.0	0.060	55	0.887
11	007	LSC-59-60 @ 400C	200°C, 19 barg, 9 l/h	28.7	27.4	15.3	27.8	0.6	0.2	0.0	0.35	2.5	5.8	0.70	test run	3.01	1.02	60.0	0.049	53	0.873
12	007	LSC-59-60 @ 400C	220°C, 19 barg, 9 l/h	36.0	29.0	15.1	19.7	0.0	0.1	0.0	0.43	12.9	18.0	0.56	test run	3.01	1.02	60.0	0.049	53	0.873
13	008	ALD12 - 5 cy Al2O3	200°C, 19 barg, 9 l/h	52.5	0.3	0.3	0.2	0.0	0.0	46.6	0.53	81.9	85.1	0.71	test run	0	0.93	43.1	0.000		
14	008	ALD12 - 5 cy Al2O3	220°C, 19 barg, 9 l/h	54.6	0.8	0.4	0.5	0.0	0.0	43.7	0.43	73.9	80.6	0.58	test run	0	0.93	43.1	0.000		
15	009	ALD9 - 5 cy Al2O3	200°C, 19 barg, 9 l/h	58.0	0.6	0.4	0.7	0.0	0.0	40.3	0.35	68.7	79.6	0.72	test run	0	0.93	43.1	0.000		
16	009	ALD9 - 5 cy Al2O3	220°C, 19 barg, 9 l/h	38.9	24.4	18.9	17.1	0.5	0.2	0.0	0.52	11.9	18.7	0.62	test run	0	0.93	43.1	0.000		
17	010	ALD8 - 20 cy Al2O3	220°C, 19 barg, 9 l/h	35.9	22.1	22.3	18.7	0.4	0.5	0.0	0.54	9.4	15.2	0.72	test run	3.79	0.99	71.2	0.054	49	0.881
18	010	ALD8 - 20 cy Al2O3	200°C, 19 barg, 9 l/h	23.8	15.9	31.6	22.8	4.8	1.2	0.0	0.58	0.5	6.2	0.97	test run	3.79	0.99	71.2	0.054	49	0.881
19	010	ALD8 - 20 cy Al2O3	230°C, 19 barg, 9 l/h	41.9	23.3	18.4	15.6	0.6	0.2	0.0	0.54	20.1	26.9	0.61	test run	3.79	0.99	71.2	0.054	49	0.881
20	011	ALD7 - 20 cy Al2O3	220°C, 19 barg, 9 l/h	34.1	25.3	19.5	19.8	0.5	0.8	0.0	0.50	6.4	13.1	0.68	test run	1.64	0.98	71.2	0.024	47	0.839
21	011	ALD7 - 20 cy Al2O3	200°C, 19 barg, 9 l/h	27.2	21.4	24.5	23.4	2.0	1.4	0.0	0.51	-1.3	4.5	0.83	test run	1.64	0.98	71.2	0.024	47	0.839
22	011	ALD7 - 20 cy Al2O3	230°C, 19 barg, 9 l/h	41.3	15.2	6.6	3.5	0.0	0.0	33.4	0.65	58.9	65.3	0.42	test run	1.64	0.98	71.2	0.024	47	0.839
23	012	ALD10 - 40 cy Al2O3	220°C, 19 barg, 9 l/h	34.2	21.1	19.0	24.0	1.0	0.7	0.0	0.44	9.5	15.4	0.75	test run	3.7	1.07	72.8	0.047	54	0.907
24	012	ALD10 - 40 cy Al2O3	200°C, 19 barg, 9 l/h	28.6	24.8	24.9	19.8	0.7	1.1	0.0	0.56	0.2	7.5	0.77	test run	3.7	1.07	72.8	0.047	54	0.907
25	013	ALD13 - 5 cy Pt	220°C, 19 barg, 9 l/h	35.0	26.1	22.8	15.0	0.4	0.7	0.0	0.60	8.1	14.7	0.70	test run	2.03	1.02	72.8	0.027	46	0.858
26	013	ALD13 - 5 cy Pt	200°C, 19 barg, 9 l/h	28.6	24.6	25.1	19.8	0.7	1.2	0.0	0.56	-0.2	6.7	0.78	test run	2.03	1.02	72.8	0.027	46	0.858
27	-	LSC59-60	-	-	-	-	-	-	-	-	-	-	-	-	preparation	-	-	-	-	-	-
28	-	LSC61	-	-	-	-	-	-	-	-	-	-	-	-	preparation	-	-	-	-	-	-
29	-	R-1	-	-	-	-	-	-	-	-	-	-	-	-	preparation	-	-	-	-	-	-
30	-	R-1	-	-	-	-	-	-	-	-	-	-	-	-	preparation	-	-	-	-	-	-
31	-	ALD10 - 40 cy Al2O3	-	-	-	-	-	-	-	-	-	-	-	-	preparation	-	-	-	-	-	-
32	-	ALD13 - 5 cy Pt	-	-	-	-	-	-	-	-	-	-	-	-	preparation	-	-	-	-	-	-
33	-	ALD13 - 5 cy Pt	-	-	-	-	-	-	-	-	-	-	-	-	preparation	-	-	-	-	-	-
34	-	Puralox	-	-	-	-	-	-	-	-	-	-	-	-	base material	-	-	-	-	-	-
35	-	ALD11 - 40 cy Al2O3	-	-	-	-	-	-	-	-	-	-	-	-	preparation	-	-	-	-	-	-
36	-	ALD7 - 20 cy Al2O3	-	-	-	-	-	-	-	-	-	-	-	-	preparation	-	-	-	-	-	-
37	-	ALD12 - 5 cy Al2O3	-	-	-	-	-	-	-	-	-	-	-	-	preparation	-	-	-	-	-	-

Table 5. Compilation of data obtained for all experimental runs, post-run and pre-run characterization (part 2)

APPENDIX 2 (2/2)

			Optical	BET	XRF (Atomic%)					EDS surface (Atomic%)						EDS core (Atomic%)					
#	Run	Sample	Ellipsometry	BET Area (m2/g)	O	Co	Al	Si	Pt	O'	Co'	Al'	Si'	Pt'	EDS-comment	O"	Co"	Al"	Si"	Pt"	EDS-comment
1	002	ALD6 - 20 cy Al2O3	5.1																		
2	002	ALD6 - 20 cy Al2O3	5.1																		
3	002	ALD6 - 20 cy Al2O3	5.1																		
4	003	LSC-59-60																			
5	003	LSC-59-60																			
6	003	LSC-59-60																			
7	004	LSC-59-60 @ 400C																			
8	005	LSC-59-60 @ 300C																			
9	006	LSC-59-60 @ 300C																			
10	006	LSC-59-60 @ 300C																			
11	007	LSC-59-60 @ 400C		21.38						39.4	38.7	21.5	0.2	0.2	normal	54.4	5.5	39.3	0.8	0	normal
12	007	LSC-59-60 @ 400C		21.38																	
13	008	ALD12 - 5 cy Al2O3	3.45																		
14	008	ALD12 - 5 cy Al2O3	3.45																		
15	009	ALD9 - 5 cy Al2O3	3.65		38.1	32	28.5	0.628	0.255												
16	009	ALD9 - 5 cy Al2O3	3.65		38.1	32	28.5	0.628	0.255												
17	010	ALD8 - 20 cy Al2O3	6		37.8	32.8	27.8	0.625	0.276												
18	010	ALD8 - 20 cy Al2O3	6		37.8	32.8	27.8	0.625	0.276												
19	010	ALD8 - 20 cy Al2O3	6		37.8	32.8	27.8	0.625	0.276												
20	011	ALD7 - 20 cy Al2O3	14																		
21	011	ALD7 - 20 cy Al2O3	14																		
22	011	ALD7 - 20 cy Al2O3	14																		
23	012	ALD10 - 40 cy Al2O3	8.65																		
24	012	ALD10 - 40 cy Al2O3	8.65																		
25	013	ALD13 - 5 cy Pt	4.6		36.2	33	24.2	1.38	4.64												
26	013	ALD13 - 5 cy Pt	4.6		36.2	33	24.2	1.38	4.64												
27	-	LSC59-60		53.506	37.2	35.3	26.4	0.411	0.301	54.2	35.4	10.1	0.2	0.1		57.6	6.8	34.6	0.9	0	
28	-	LSC61		70.5681						55.4	28.6	15.3	0.7	0		60.7	4.2	33.1	2	0	
29	-	R-1		105.2005	39.5	30.7	27.8	1.49	0	55.8	16.9	26	1.4	0	normal	59.3	3.1	35.3	2.3	0	normal
30	-	R-1		105.2005	39.5	30.7	27.8	1.49	0	29.8	63.5	6.4	0.3	0	co-heavy	30	49.2	19.5	1.3	0	light-ext
31	-	ALD10 - 40 cy Al2O3	8.65		38.1	32	28.9	0.314	0.279												
32	-	ALD13 - 5 cy Pt	4.6	63.289	37.3	29.2	27.1	1.26	4.57	57.3	12.4	26.5	1.2	2.6	pt-heavy	59.7	5.5	32.8	2	0	
33	-	ALD13 - 5 cy Pt	4.6	63.289	37.3	29.2	27.1	1.26	4.57	55.2	32.6	11.2	0.6	0.3	pt-light	59.7	5.5	32.8	2	0	
34	-	Puralox		140.0196						64.4	0	35.6	0	0	homogeneous	64.4	0	35.6	0	0	same-as-external
35	-	ALD11 - 40 cy Al2O3	8.95	1.1093																	
36	-	ALD7 - 20 cy Al2O3	14	77.8204																	
37	-	ALD12 - 5 cy Al2O3	3.45	71.3049																	